(NASA-CR-161843) HIGH RESOLUTION ANGULAR SENSOR Final Report (Raytheon Co.) 108 p HC A06/MF A01 CSCL 14B

N81-31528

Unclas G3/35 27384

HIGH RESOLUTION ANGULAR SENSOR

FINAL REPORT

ER81-4177 JUNE 1981

Contract No.
NAS8-31840

Prepared for

George C. Marshall Space Flight Center
Marshall Space Flight Center
Alabama 35812

RAYTHEON COMPANY
EQUIPMENT DIVISION

RAYTHEON COMPANY
EQUIPMENT DIVISION

HIGH RESOLUTION ANGULAR SENSOR

FINAL REPORT

ER81-4177 JUNE 1981

Contract No. NAS8-31840

Prepared for

George C. Marshall Space Flight Center
Marshall Space Flight Center, Alabama 35812

Prepared by

Morris I. Gneses
Dennis S. Berg

Raytheon Company
Equipment Division
Strategic Systems Directorate
Advanced Systems
Sudbury, Massachusetts 01776

TABLE OF CONTENTS

TABLE OF CONTENTS (Cont'd)

ILLUSTRATIONS

ILLUSTRATIONS (Cont'd)

SECTION 1

INTRODUCTION AND SUMMARY

1.1 INTRODUCTION

The High Resolution Angular Sensor Contract No. NAS8-31840 was completed as of March 31, 1979. The objective of this program was to perform studies and conduct experiments to investigate the feasibility of reducing ring laser gyro output quantization to the sub-arc-second level by the use of phase locked loops and associated electronics. Raytheon's existing Multioscillator Laser Gyro patents (No.'s 3,741,657 and 3,854,819) were to be used as the stimulus to demonstrate this phase locked loop concept.

Prior work by Raytheon on IDP funds had resulted in a reduction to practice of a dual phase locked loop (PLL) system which formed the basis for the circuitry utilized on this contract. The final design selection was made from a variety of design options previously investigated under IDP funding. These options included single and dual loop configuration with analog, digital and hybrid mechanizations. The elements of the design selection are treated in Section 3 of this report. Section 4 covers the final electrical design which was utilized during the test phases.

Two separate ring laser multioscillator gyros were used for testing the high resolution concept. The initial testing was conducted with an RB-55-1 (55 cm path length) gyro which had a nominal pulse quantization of 0.8 arc-seconds. The voltage controlled crystal oscillators (VCXO's) used in the PLL's had a center frequency of 70MHz (which was effectively shifted to 65 MHz to achieve some bias offset control) which with the Faraday bias frequenices of the RB-55 gyro allowed a quantization reduction by 364 to 0.0022 arc-seconds.

After the initial testing with the RB-55 gyro it developed a non-repairable defect and had to be replaced by an RB-25-11 (25 cm path length) gyro which had a nominal quantization of 1.5 arc-seconds but basically 5 times the Faraday bias frequency of the RB-55. With the fixed oscillator frequency (65 MHz), previously set, only a quantization reduction by a factor of 72 to 0.022 arc-seconds was achievable with the replacement RB-25 gyro. This is not an inherent limitation since the quantization reduction is governed by the ratio of the VCXO center frequency to the Faraday bias frequency and a proper choice of VCXO center frequency will give any desired resolution capability that is meaningful in terms of basic sensor accuracy.

The contract effort was essentially broken into two phases. In the initial (or Phase I) effort a dual PLL breadboard was constructed (see Section 4 for details) with a quantization capability, with the Raytheon RB-55 laser gyro initially tested, of 0.0022 arc-seconds. At the end of the Phase I effort a demonstration test was conducted in which the gyro was mounted on a floating table. Small motions (less than an arc-second) were imparted to the table in an azimuth sense by suspending a pendulum on the bottom of the table. These motions, which were below the nominal quantization (0.8 arc-seconds) of the gyro, were easily detected by use of the high resolution circuits. Refer to Section 5 for actual test results. The success of the demonstration test resulted in Raytheon being funded to extend its testing with monitoring equipment supplied by NASA. It was the intent of this follow-on effort (referred to herein as Phase II) to check the gyro results at low frequency with a tiltmeter which would monitor the seismic background. This type of test did not turn out to be feasible due to a lowly damped resonant mode, at a frequency of 0.2 cps, in the tiltmeter. The tiltmeter was a dual mercury reservoir type manufactured in 1969 by Ideal-Aerosmith. The resonant

effect was due to the interchange of mercury between the two cisterns of the device which acted as two variable capacitances in a balanced bridge arrangement with two fixed capacitances. The tiltmeter was also responsive to personnel approaching the device and capacitively coupling into the bridge. In the light of these limitations a new test approach was called for as discussed below.

In the new approach the gyro was mounted with its sensitive axis in the local horizontal plane. In this position the gyro was placed on a granite surface plate which rested freely, supported on three pads, on a metal support structure. Nearest the front single pad a differential screw (with a high mechanical advantage) was attached to the metal support frame. To the top of the screw was appended a PZT. By hand-pressure the screw could be turned to push the PZT into contact with the bottom of the surface plate with an adjustable pre-load. With this arrangement we were able to oscillate the plate about the horizontal axis using a high voltage supply (1 Kv). A function generator was used to control the supply voltage to give the desired amplitudes and frequencies of angular motion. With this set-up we were able to oscillate the surface plate at a few hundreths of an arc-second up to as high as 1.4 arc-seconds at a peak voltage of 900 volts. At low voltages frequencies as high as 65 Hertz were tried.

In spite of the monitoring difficulties we were able, in the Phase II tests, to show substantial sensitivity to low amplitude angular motions of the order of the resolution (0.022 arc-seconds). As will be explained in detail in Section 5, we were able to sense motions beyond the basic bandwidth of the phase locked loops (10 Hertz). These motions are attributable to structural resonances of the surface plate support structure occuring in the 10 to 100 Hertz frequency band. We were able to see changes in the resonant fre-

quency by changing the stiffness of the front support pad. With the normal support a resonance was sensed at approximately 52 Hertz. By jacking up the table and inserting two layers of iso-padding we were able to shift the resonance down in frequency to approximately 40 Hertz. At the same time we were able, with the PZT, to get an increase in peak-to-peak angular motion from 0.8 arc-seconds to 1.4 arc-seconds at frequencies within the bandwidth of the PLL's.

To set a high resolution design goal we started the Phase I effort using the specifications for the pointing stabilization system of the LST (Large Space Telescope) program. These specifications are introduced in Section 2.1 prior to a discussion of the system analysis effort.

1.2 SUMMARY

The system analysis procedures are discussed in Section 2. It is shown in this section that a first order loop filter, resulting in a second order closed loop, can meet the measurement noise requirements when the loop gain and time constant of the loop filter are appropriately chosen. The highest Large Space Telescope (LST) rate accuracy requirement can be met with the oscillators chosen for the phase locked loops. A multioscillator laser gyro model is presented along with data on the oscillator noise. An examination is also given of the response of the phase locked loop to the gyro and oscillator noise processes.

Section 3 covers the preliminary electrical design from the standpoint of circuit tradeoff considerations. Analog, digital and hybrid designs are given and their applicability to the high resolution sensor is discussed.

The final electrical design choice of a system configuration is detailed in Section 4. The design and operation of the various modules is also covered in this section. Also included, for completeness, are the system block diagrams.

Section 5 goes into the system testing effort. Coverage is given to noise floor testing of the PLL electronics in Section 5.2. In Section 5.3 we present the Phase I demonstration test results using the RB-55-1 multioscillator laser gyro interfaced to the high resolution phase locked loops. Section 5.4 goes into the Phase II testing. The latter tests were conducted with the RB-25-11 laser gyro operating on a surface plate which could be oscillated about a horizontal axis using a PZT driver to input small angular test motions.

Analysis and design details are relegated to the six appedices at the end of the report.

SECTION 2

SYSTEM ANALYSIS

2.1 INTRODUCTION

Many considerations enter into the system design of a high resolution angular sensor. To proceed on a logical footing the specifications for the pointing stabilization system for the LST (Large Space Telescope) were used as a goal. In the LST program pointing stabilities of the order of 0.005 arc-seconds are being sought for the overall system with 0.001 arc-seconds being budgeted for the rate gyro contribution to the system performance. Rate noise requirements for the gyro have also been studied (Ref. 2-1). The gyro was assumed to have a white noise PSD (power spectral density) ranging from 6.0×10^{-5} to 2.4×10^{-4} (micro-radians/sec)^2/Hz or 2.55×10^{-6} to 1.02×10^{-5} (arc-sec/sec)^2/Hz.

In Section 2.2 a model is postulated for the multioscillator laser gyro which includes, in addition to quantization error, random noise originating from the spontaneous emission process. Section 2.3 is a discussion of the predominant source of noise in the PLL electronics arising from the frequency stability characteristics of the voltage controlled crystal oscillators. Section 2.4 contains detailed work on the response of the phase locked loops to noise.

2.2 LASER GYRO MODEL

Both two-frequency and four-frequency (multioscillator) laser gyros have rate errors due to the pulse quantization of a specific gyro's digital output. Other than this quantization error, the prime error in two-frequency gyros is a white noise rate error

which arises from the dithering process. The latter error is not present in the multioscillator laser gyro. Based upon a study of the technical literature we offer the tentative theory that the multioscillator gyro has an ultimate accuracy that is limited by the spontaneous emission process of the laser.

2.2.1 LASER GYRO QUANTIZATION ERROR

The nature of the rate error due to pulse quantization of the laser gyro's digital output was examined in Reference 2-2 and is repeated in Appendix A for convenience. The rate error due to gyro quantization is

$$\sigma_q = \frac{\Delta\theta}{\sqrt{6}\ T}$$

where $\Delta\theta$ is the pulse quantization angle and T is the interval over which the pulses are summed.

The gyro being used to test the high resolution concept is designated the RB-55 (55 cm pathlength) and has a $\Delta\theta$ = 0.8 arc-seconds. The rate error due to the latter value is shown on the plot of Figure 2-1 along with the rate error bounds required by the LST program. The experimental PLL system has a resolution ratio of 364 for an equivalent $\Delta\theta$ = 0.0022 arc-seconds. The rate quantization error for this high resolution case is also shown in Figure 2-1.

2.2.2 LASER GYRO SPONTANEOUS EMISSION ERROR

Sources of noise in laser oscillators are spontaneous emission noise and thermal (Johnson) noise. Yariv (Reference 2-3) has shown that the thermal noise may be neglected relative to the spontaneous emission noise. Work by Raytheon researchers and consultants (Reference 2-4) has indicated that for a single mode laser, the random frequency fluctuation can be written as,

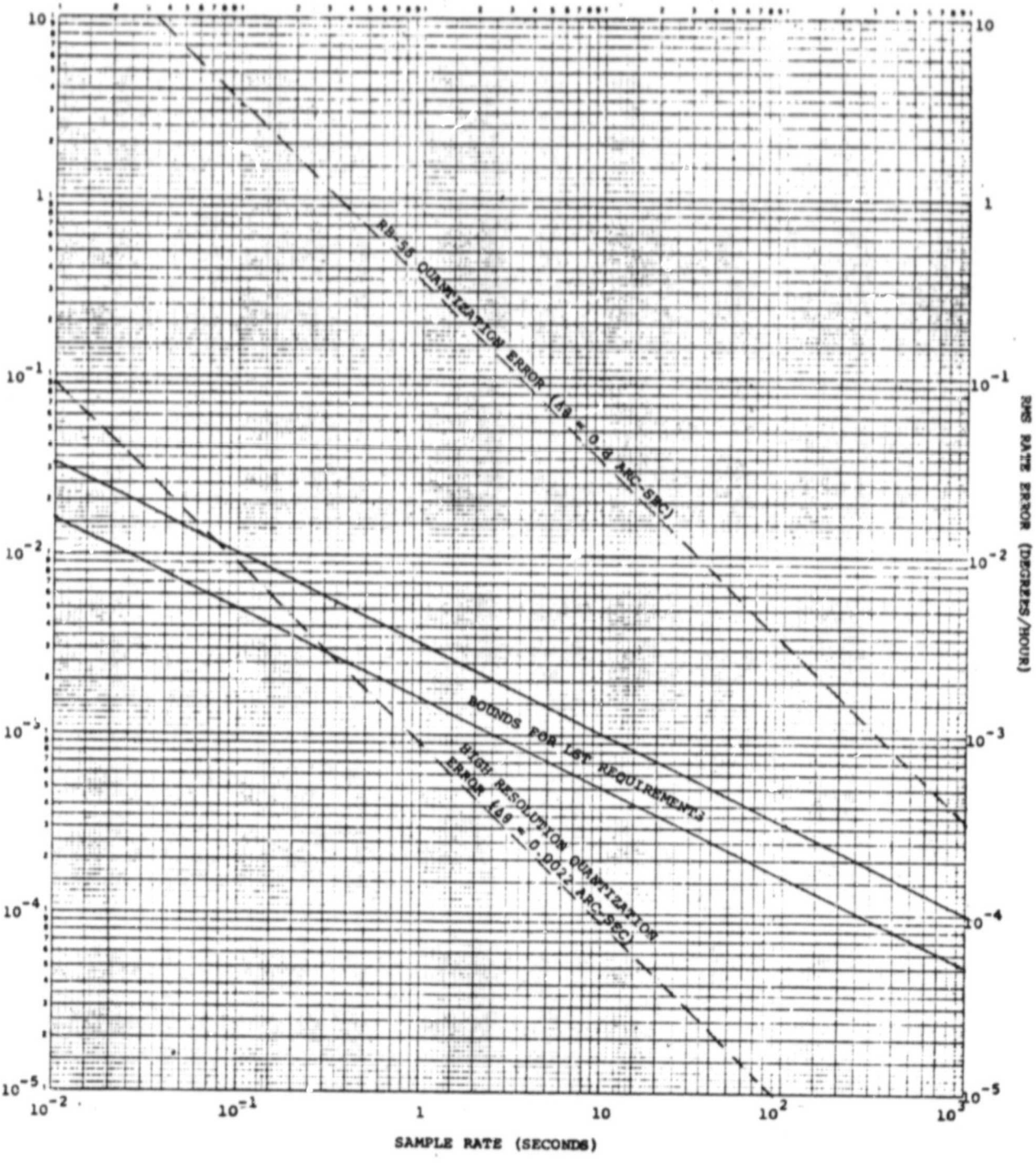

Figure 2-1. Comparison of Quantization Error & Gyro Accuracy Requirements for LST

$$\Delta f = \left[\left(\frac{\nu_o}{Q}\right)^2 \frac{h\nu_o}{P_{el}} B\right]^{1/2}$$

where

h = Planck's constant = 6.63×10^{-34} watt sec^2

ν_o = Light frequency = 4.73×10^{14} Hz (for He-Ne laser)

Q = Quality factor of cavity

P_{el} = Power dissipated in cavity (single mode)

B = Frequency processing bandwidth.

For a four frequency laser gyro we would have

$$\Delta f = \frac{4\nu_o}{Q} \left[\frac{h\nu_o}{P_e} B\right]^{1/2}$$

$$P_e = \sum_{i=1}^{4} P_{ei} = P_{out}\, \alpha/t = P_c \alpha$$

where

α = Cavity loss

t = Transmissivity of output mirror

P_{out} = Total output power

P_c = Total circulating power in cavity.

An approximate bandwidth of $B = 1/2T$ can be assumed where T is the averaging time for the frequency measurement. Also for a non-planar cavity it can be shown that (assuming an index of refraction = 1),

$$\frac{\nu_o}{Q} = \frac{\alpha c}{2\pi L}$$

where

c = Speed of light = 3×10^{10} cm/sec

L = Length of ring cavity perimeter.

Thus for the helium-neon four-frequency gyro we have that,

$$\Delta f = \frac{7.57}{L} \left(\frac{\alpha}{P_c}\right)^{1/2} \frac{1}{\sqrt{T}}.$$

The above expression can be converted to rms rate by multiplying by the scale factor S

$$\Delta \text{rate} = \Delta R = \frac{7.57S}{L}\left(\frac{\alpha}{P_c}\right)^{1/2}\frac{1}{\sqrt{T}}$$

$$S = \frac{\lambda L}{8A} = \frac{cL}{8\nu_o A}$$

where A is the enclosed area of the ring.

If we consider equilateral triangular rings, we find that

$$A = \frac{L^2}{12\sqrt{3}}$$

which leads to (for rate expressed in degrees/hour)

$$S = \frac{34}{L} .$$

Substitution into the ΔR expression finally gives

$$\Delta R = \frac{257}{L^2}\left(\frac{\alpha}{P_c}\right)^{1/2}\frac{1}{\sqrt{T}}$$

where ΔR will be in degrees per hour for L in cm, P_c in watts and T in seconds.

If we use the white noise PSD from Ref. 2-1 of $2.55\text{x}10^{-6}$ $(\text{degrees/hour})^2/\text{Hz}$,

$$\Delta R = \left[\frac{2.55\text{x}10^{-6}}{T}\right]^{1/2} = \frac{1.60\text{x}10^{-3}}{\sqrt{T}}$$

where R will be in degrees per hour for T in seconds. If now equate this to the previous expression for R we have that

$$P_c = 2.58\text{x}10^{10}\ \alpha/L^4 .$$

The latter expression defines the relationship between the parameters P_c, α and L required to meet the most accurate LST requirement. The above expression is plotted in Figure 2-2 for various cavity path lengths assuming an equilateral triangular geometry for the cavity. Cavity parameters on or above a line corresponding to the gyro path length will meet or exceed the most accurate LST gyro noise requirement.

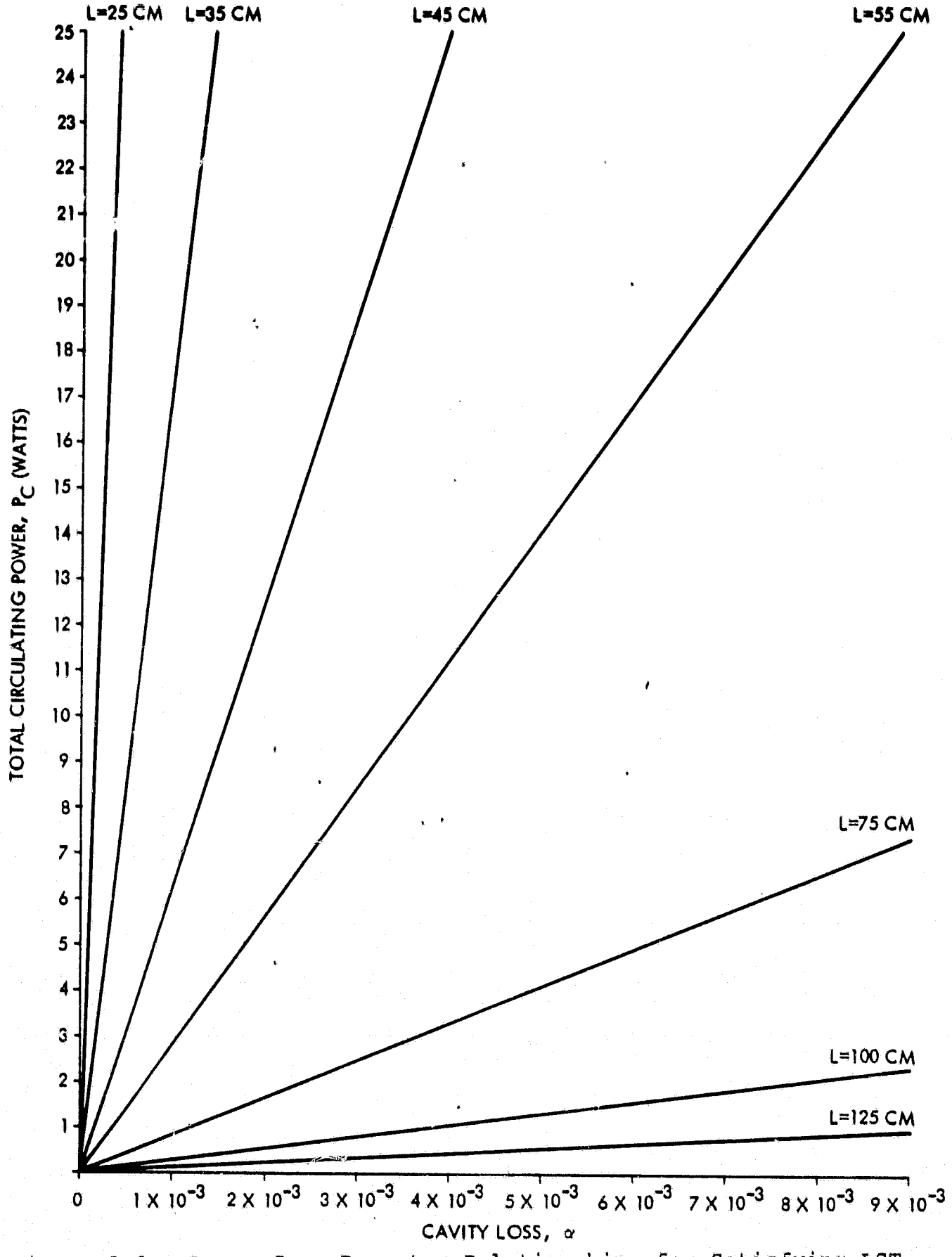

Figure 2-2. Laser Gyro Paramter Relationships for Satisfying LST Requirement

2.3 VOLTAGE CONTROLLED CRYSTAL OSCILLATOR NOISE

From the standpoint of low noise the best oscillators to use in the PLL electronics are high Q crystal oscillators. It should be noted however that high stability (low noise) oscillators have restricted frequency pulling capabilities. Thus the higher the stability the less the frequency pull range. An analysis of the relationship between frequency stability and frequency pull range is presented in Appendix B.

High precision VCXO's are not off-the-shelf components. Exact specifications must be prepared and two to three month delivery schedules are typical. Since the high resolution system is of an experimental type and in order to expedite the fabrication of equipment it was decided to use internally available high precision VCXO's.

The noise of these oscillators has been measured in the time domain using the short-term stability technique (also referred to as the Allan Variance or Fractional Frequency Deviation method). The test equipment utilized was the Hewlett-Packard 5360A Computing Counter. Details of the measurement technique and specifics on the Computing Counter can be found in Appendix C.

The short term stability data taken with the Computing Counter on two 70 MHz VCXO's is shown in Figure 2-3. It is shown in Section 2.4 that the short-term stability of these oscillators is better (by an order of magnitude) than needed to meet the LST requirements.

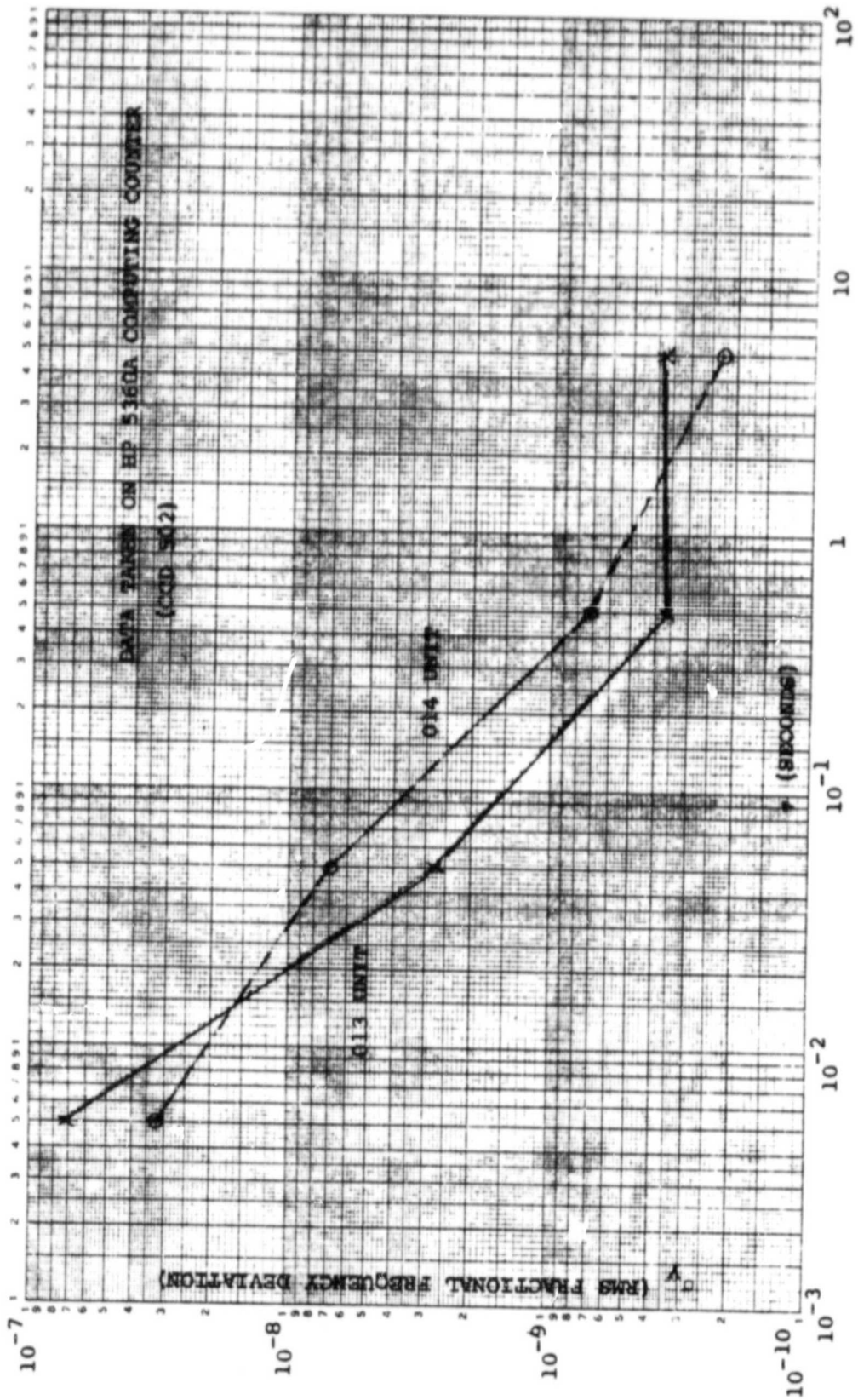

Figure 2-3. Short Term Stability of 70 MHz VCXO's

2.4 PHASE LOCKED LOOP RESPONSE TO NOISE

The response of the PLL may be optimized for various loop filters and for combinations of noise disturbances originating in the gyro and/or gyro electronics and the VCXO. The response of a second order PLL is analyzed below.

Consider the loop structure given in Figure 2-4. A first order loop filter is assumed with the unity gain transfer function $1/(\tau_1 S + 1)$. Three separate disturbances are considered to perturb the loop,

(a) a laser gyro frequency modulation such as the spontaneous emission type discussed in Section 2.2

(b) a VCXO frequency modulation (see Section 2.3)

(c) an additive noise on the laser gyro signal.

The disturbances (a) and (b) are representable as white noises [with constant power spectral densities (PSD's)] for the reasons discussed above. The input signal (laser gyro signal) is given by $y(t) = A \sin(\omega t + \theta) + n(t)$ where $n(t)$ is the additive noise. If the frequency band is narrow and symmetrical with respect to the central frequency, the noise process $n(t)$ can be modeled as:

$$n(t) = n_1(t) \sin \omega t + n_2(t) \cos \omega t$$

where $n_1(t)$ and $n_2(t)$ are low-frequency random processes which are Gaussian, stationary and statistically independent. These processes have two-sided PSD's N_o that are uniform in the frequency band say $-W/2$ to $+W/2$. In this case we have that

$$\overline{n_1^2(t)} = \overline{n_2^2(t)} = \overline{n^2(t)} = N_o W.$$

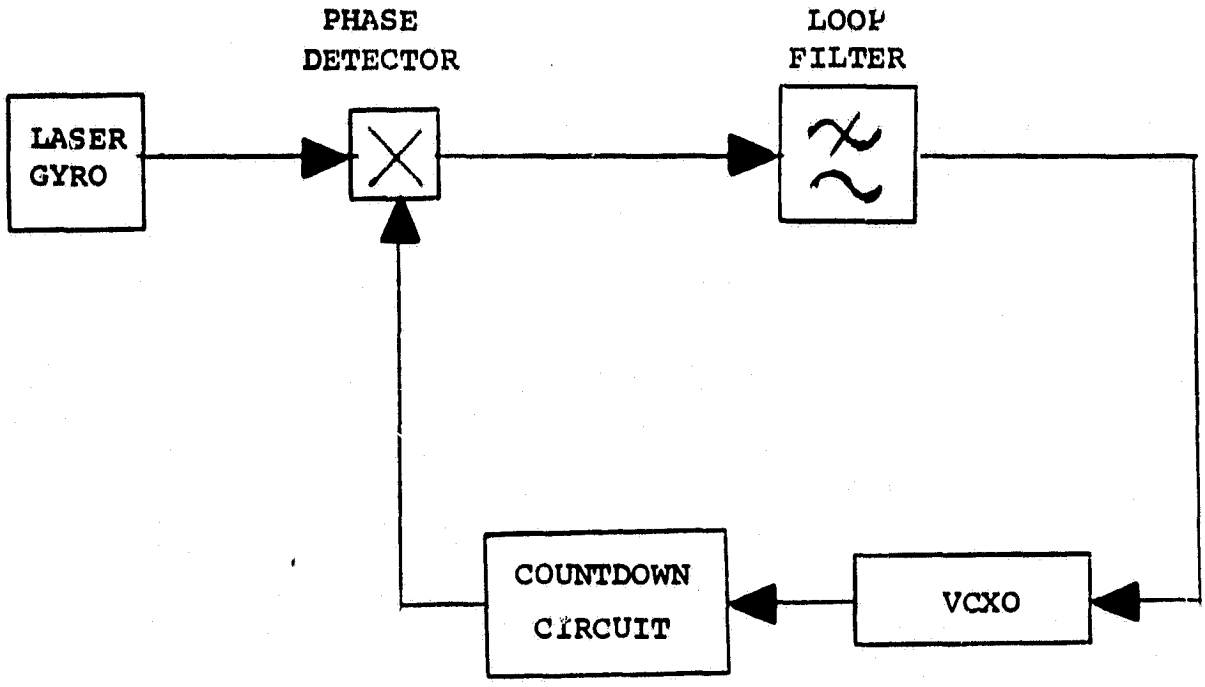

LOOP FILTER TRANSFER FUNCTION: $\frac{1}{\tau_1 S + 1}$

Figure 2-4 Phase Locked Loop Block Diagram

Let us determine the mean-square value ($\sigma^2_{\phi e}$) of the phase error for the PLL, Let H(S) be the transfer function $\phi_o(S)/\phi_i(S)$,

$$H(S) = \frac{K}{\tau_1 S^2 + S + K}$$

where K is the open-loop gain. In terms of damping ratio (ζ) and natural frequency (ω_n),

$$H(S) = \frac{\omega_n^2}{S^2 + 2\zeta\,\omega_n S + \omega_n^2} \quad .$$

It can be shown that the PSD of the phase error (S_{ϕ_e}) is given by

$$S_{\phi_e} = (S_{\phi_a} + S_{\phi_b})|1 - H(j\omega)|^2 + S_c|H(j\omega)|^2.$$

Let $S_{\phi_a} = N_a$ and $S_{\phi_b} = N_b$ with white noise frequency modulation of the gyro and VCXO, respectively. Therefore,

$$S_{\phi_a} = \frac{(2\pi)^2 N_a}{\omega^2}$$

$$S_{\phi_b} = \frac{(2\pi)^2 N_b}{\omega^2} \quad .$$

Thus S_{ϕ_e} becomes

$$S_{\phi_e} = (2\pi)^2 (N_a + N_b) \left[\frac{-\omega + j\, 2\zeta\, \omega_n}{-\omega^2 + j\, 2\zeta\, \omega_n\, \omega + \omega_n^2} \right] \left[\text{conjugate} \right]$$

$$+ S_C\, \omega_n^4 \left[\frac{1}{-\omega^2 + j\, 2\zeta\, \omega_n\, \omega + \omega_n^2} \right] \left[\text{conjugate} \right] .$$

The mean-square phase error is given by

$$\sigma_{\phi_e}^2 = -2\pi\, (N_a + N_b) \int_{-\infty}^{\infty} d\omega \left[\frac{-\omega + j\, 2\zeta\, \omega_n}{-\omega^2 + j\, 2\zeta\, \omega_n\, \omega + \omega_n^2} \right] \left[\text{conjugate} \right]$$

$$+ \left(\frac{S_C\, \omega_n^4}{2\pi} \right) \int_{-\infty}^{\infty} d\omega \left[\frac{1}{-\omega^2 + j\, 2\zeta\, \omega_n\, \omega + \omega_n^2} \right] \left[\text{conjugate} \right] .$$

Expressions such as these may be evaluated using special tables (see Reference 2-5). The term with the first integral evaluates to

$$I_1 = \frac{\pi^2 (1 + 4\zeta^2)}{\zeta\, \omega_n} (N_a + N_b) .$$

The term containing the second integral evaluates to

$$I_2 = \left(\frac{S_C\, \omega_n^4}{2\pi} \right) \left(\frac{\pi}{2\zeta\, \omega_n^3} \right) = \frac{S_C\, \omega_n}{4\zeta} .$$

If the additive noise model discussed above is used with a sinusoidal type phase detector then

$$\upsilon_C = \frac{N_o}{A^2}$$

where A is the input amplitude. Thus the mean-square phase error is

$$\sigma^2_{\phi_e} = \frac{(N_a + N_b)\pi^2(1 + 4\zeta^2)}{\zeta\, \omega_n} + \left(\frac{N_o}{A^2}\right)\left(\frac{\omega_n}{4\zeta}\right) .$$

If we assume that the damping ratio can be chosen, $\sigma^2_{\phi_e}$ is a minimum when the two terms are equal. Therefore (if the optimum ω_n is denoted by ω_n^o we have

$$\left(\sigma^2_{\phi_e}\right)_{min} = \frac{2(N_a + N_b)\pi^2(1 + 4\zeta^2)}{\zeta\, \omega_n^o} = 2\left(\frac{N_o}{A^2}\right)\left(\frac{\omega_n^o}{4\zeta}\right)$$

or

$$\omega_n^o = 2\pi\sqrt{1 + 4\zeta^2}\left(\frac{A}{\sqrt{N_o}}\right)\sqrt{N_a + N_b} .$$

Substituting ω_n^o back in we get that

$$\left(\sigma^2_{\phi_e}\right)_{min} = \pi\left(\frac{\sqrt{1 + 4\zeta^2}}{\zeta}\right)\left(\frac{\sqrt{N_o}}{A}\right)\sqrt{N_a + N_b} .$$

The most judicious choice of ζ turns out to be a value in the vicinity of 1. Taking $\zeta = 1$, we have

$$\left(\sigma^2_{\phi_e}\right)_{min} = \sqrt{5}\,\pi\left(\frac{\sqrt{N_o}}{A}\right)\sqrt{N_a + N_b}\ .$$

Let us now examine the noise floor of the PLL in terms of rate for oscillator frequency modulation noise. In this case the transfer function from actual rate (Ω) to indicated analog rate (ω_{IND}) is given by

$$\frac{\omega_{IND}(S)}{\Omega(S)} = \frac{\omega_n^2}{S^2 + 2\zeta\,\omega_n\,S + \omega_n^2}\ .$$

Using the technique above we find that

$$\sigma^2_{\omega_{IND}} = \left(\frac{\pi\,\omega_n}{2\zeta}\right) N_b\ .$$

Considering the equivalent digital indicated rate as being processed through a low pass filter with the transfer function $1/(\tau_2\,S + 1)$ and taking $\zeta = 1$ we have that,

$$\sigma^2_{\omega} = \left(\frac{\pi\,\omega_n}{2}\right) N_b\,\frac{(1 + 2\,\tau_2\,\omega_n)}{(1 + \tau_2\,\omega_n)^2}\ .$$

In our frequency range of interest we may approximate this as

$$\sigma^2_{\omega} \cong \frac{\pi}{\tau_2}\,N_b\ .$$

In terms of high resolution rate with N the resolution factor,

$$\left(\sigma_{\omega}\right)_{\substack{\text{HIGH} \\ \text{RESOLUTION}}} \cong \left(\frac{\sqrt{\pi}}{N}\right)\left(\frac{\sqrt{N_b}}{\sqrt{\tau_2}}\right).$$

For a typical high resolution factor (N = 364), the above relation indicates that to meet the highest LST rate accuracy requirement we require $N_b = 9 \times 10^{-2}(\text{Hertz})^2/\text{Hertz}$. The frequency modulation noise of the oscillators used in the high resolution electronics is at least an order of magnitude better than this latter value.

SECTION 3

OPTIMAL APPROACH SELECTION

Prior to an actual design effort, circuit trade-offs were made to select an optimum circuit configuration. These circuits were developed by Raytheon on IDP funds (see References 3-1, 3-2, and 3-3) and a selection from this collection was made to achieve the most suitable circuit operation. The criteria for this design were flexibility, accuracy, reliability, and operational simplicity.

3.1 SINGLE PHASE LOCKED LOOP

A single phase locked loop system was designed, fabricated and tested prior to the beginning of this contract and provided a basis for the approaches considered. A block diagram of this circuitry is shown in Figure 3-1. In this design, one of the laser gyro Faraday bias frequencies performed the function of a voltage controlled oscillator (VCO) in the phase locked loop (PLL). An active Faraday bias was achieved by placing a small solenoid over a window of the open ring test gyro. Variations in solenoid current resulted in a Faraday bias frequency variation enabling the gyro to be locked to an external frequency source. The output of this circuit is an analog voltage calibrated in arc seconds per volt.

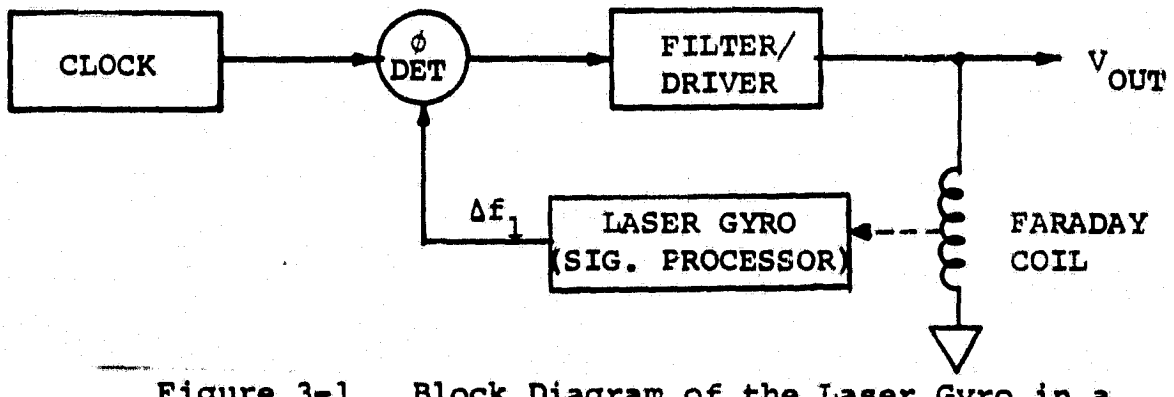

Figure 3-1 Block Diagram of the Laser Gyro in a Phase Locked Loop (PLL)

3.2 DOUBLE PHASE LOCKED LOOP

A second type of loop considered placed the Faraday bias frequency outside the loop as a signal source to which a VCO was locked. Figure 3-2 is a block diagram of two such circuits. A major advantage of this approach is that neither Faraday bias frequency is affected by the PLL circuitry. This allows the gyro to be completely isolated from the high resolution circuitry. The output is an analog voltage with units of arc seconds per volt.

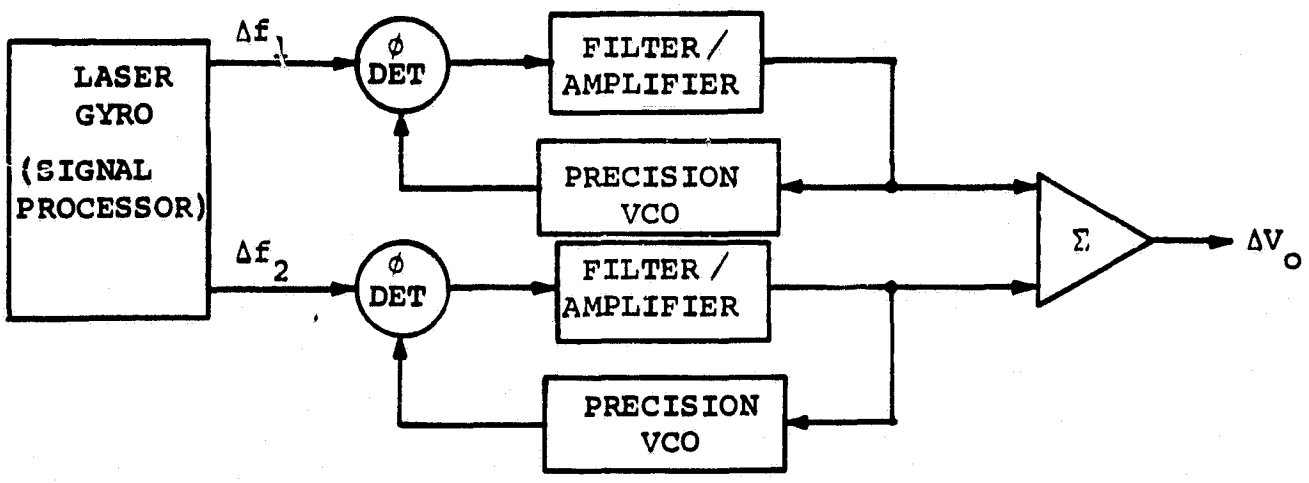

Figure 3-2 Laser Gyro Outside PLL. Double Loop Configuration Block Diagram

3.3 PHASE LOCKING TO GYRO OUTPUT

A single loop using the circuit arrangement of Figure 3-2 is shown in Figure 3-3. The gyro output difference signal, Δf (from $\Delta f_1 - \Delta f_2 = \Delta f$), is on the order of 100 - 500 Hz. It is desirable to have a crystal controlled VCO in this application. Since suitable oscillators of this type are available in the range of 50 KHz and

higher, a frequency divider is necessary to reduce its output to the Δf frequency range. The addition of the frequency divider opens the way for outputs of a different form. This is discussed in the following paragraphs. The output of this circuit is an analog voltage expressed in arc seconds per volt.

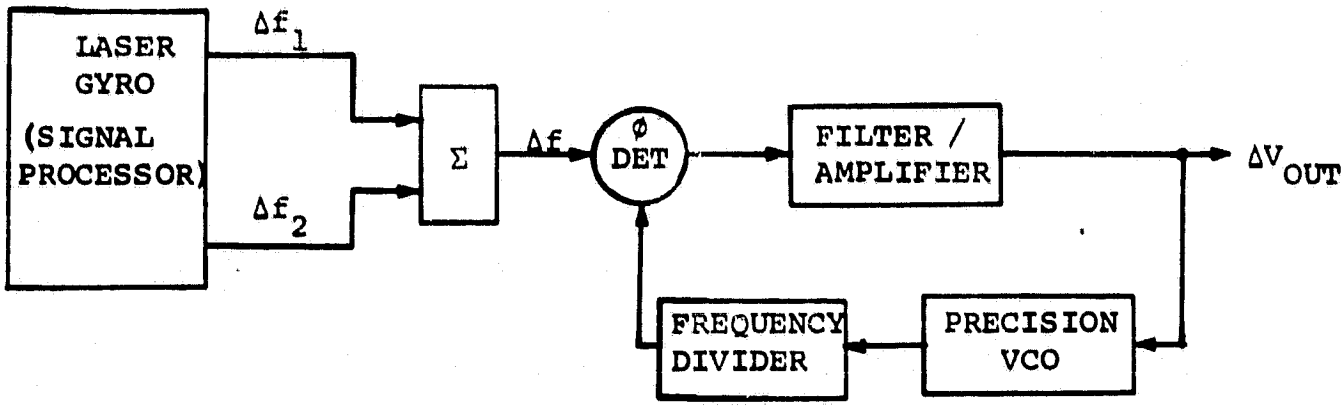

Figure 3-3 Block Diagram of VCO Locked to Difference Frequency of Two Faraday Bias Outputs

3.4 VARIATIONS OF PHASE LOCK AT OUTPUT

Two variations of the circuit of Figure 3-3 were examined. These variations are shown in Figures 3-4 and 3-5. The circuit of Figure 3-4 uses similar PLL techniques but substitutes optics for electronics to difference the two Faraday frequencies. While this simplifies the electronics required, it complicates the optics further since the gyro requires separate Faraday outputs for other reasons.

The circuit of Figure 3-5 accepts sine wave inputs from the gyro in place of the pulse trains required for previous circuits. A double-balanced mixer performs the differencing function for the PLL section. The circuit provides a choice of output form. An

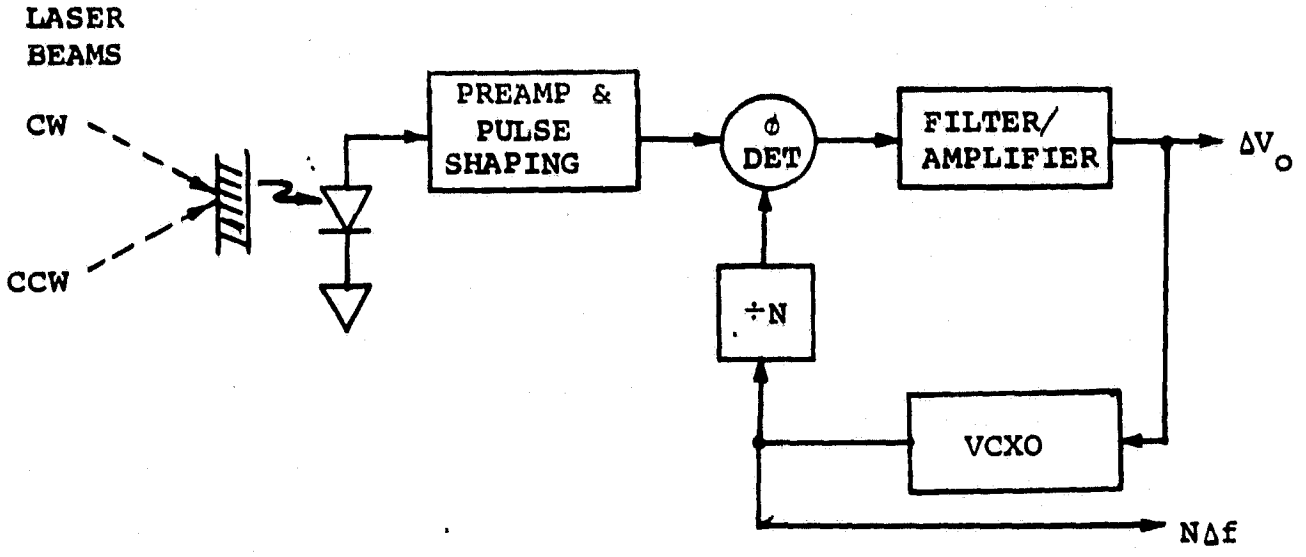

Figure 3-4 Single PLL Using Optical Mixing of Faraday Bias Signals

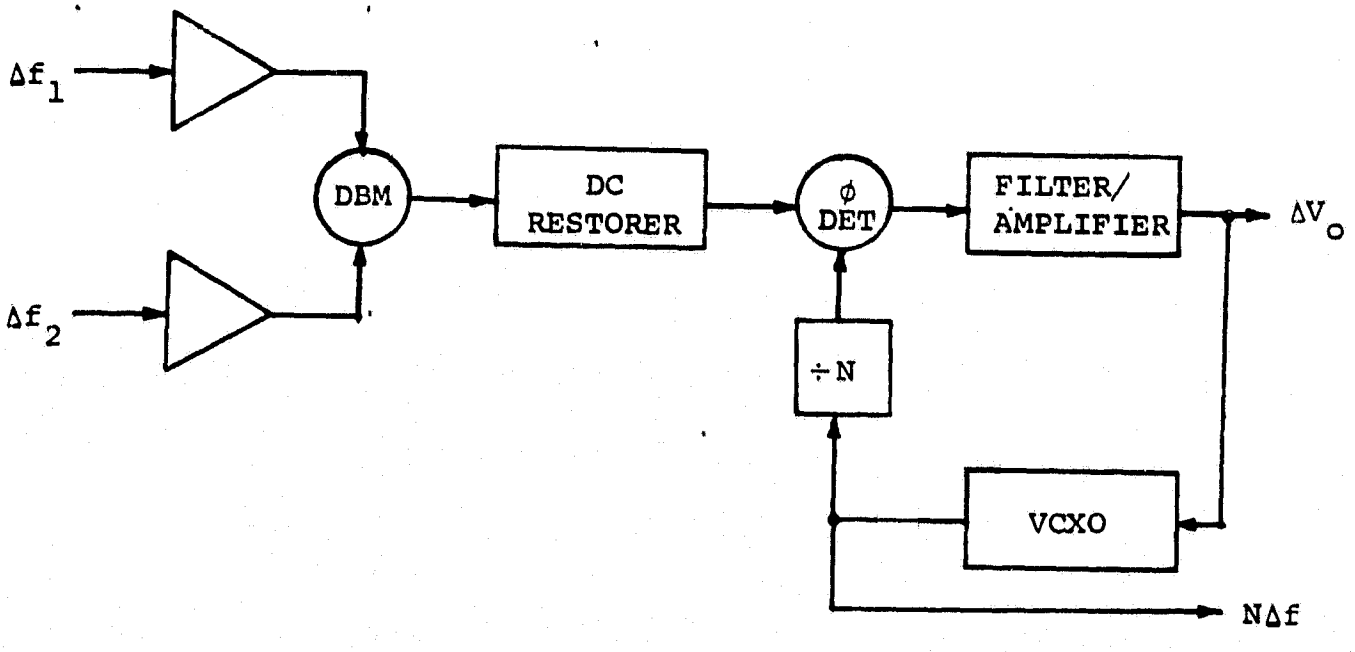

Figure 3-5 Single PLL Using Electronic Mixing of Faraday Bias Signals

analog voltage in arc seconds per volt is available and a pulse train whose frequency is proportional to rotation in arc seconds per second. The latter is related to the resolution of the gyro by the division factor, "N". The advantages of these three approaches are lower parts count, the VCO is not affected by Faraday bias frequency drift, the gyro output is unaffected and no active Faraday bias is required. However, the Faraday bias difference frequency stability is very critical.

3.5 DOUBLE PLL COMBINATION

A combination of the two loop types is shown in Figure 3-6. In this arrangement, the analog output of the Δf_1 loop is used to vary the current through the active Faraday bias coil, locking that frequency to the clock. However, the action of locking the Δf_1 bias frequency to the clock produces a frequency shift in Δf_2 of twice the magnitude during rotation. The result, then, is reflected in the analog output of the Δf_2 loop in arc seconds per volt.

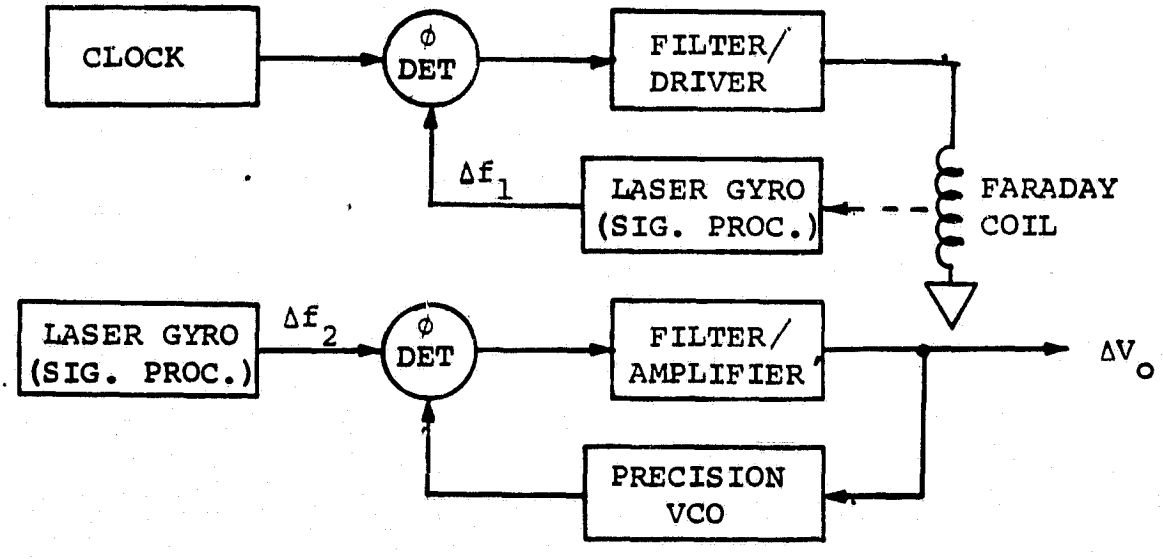

Figure 3-6 Block Diagram of Combination Laser Gyro Inside and Outside PLL

During the detailing of advantages/disadvantages and weaknesses/ strengths of each of these mechanizations of the high resolution output, it was determined that an analog rotational representation was not desirable for testing on a low rate rotation table due to line loss effects, noise, etc. Converting to digital requires another VCO which, in turn, introduces another source of error. Use of a clock to perform a digital subtraction from the VCO also incorporates a possible error source.

3.6 DIGITAL OUTPUT APPROACHES

Two approaches were considered to solve these problems. The first, shown in Figure 3-7, provides a digital word containing rotational information. The word size can be varied to meet system requirements. Also, system clock drift is cancelled through the timing gate circuitry. However, word size is difficult to change without changing the remaining circuitry.

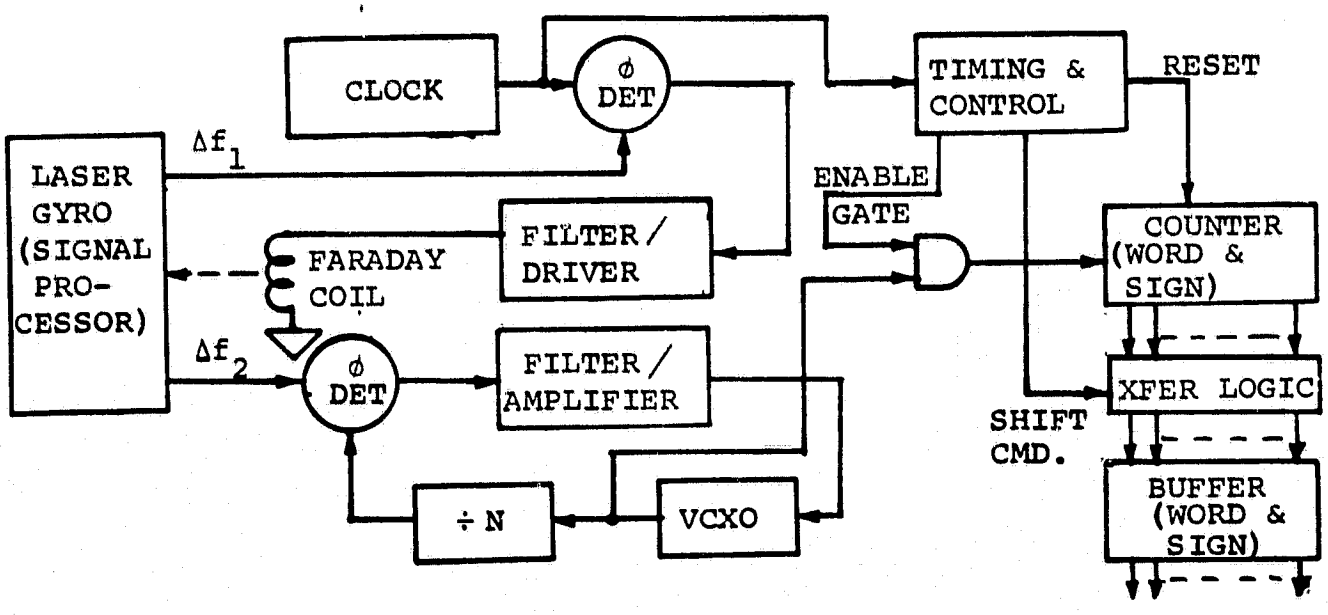

Figure 3-7 Block Diagram of Double PLL with Digital Output Word

A second solution was reached by simply adding a double-balanced mixer between two higher frequency VCO's in a double loop configuration similar to Figure 3-2. A block diagram of this circuit is shown in Figure 3-8. Loop errors in this configuration are minimized by taking advantage of loop gain, achieved by taking the pulse train output from within the phase locked loop. The accuracy of the pulse train output at any frequency becomes a function of the loop gain at that frequency. Loop gain at any frequency of interest is determined by the filter/amplifier response at that frequency. The circuit resolution becomes N times the gyro resolution. The value of N is determined by the magnitude of the Faraday bias frequency and the center frequency of the VCO.

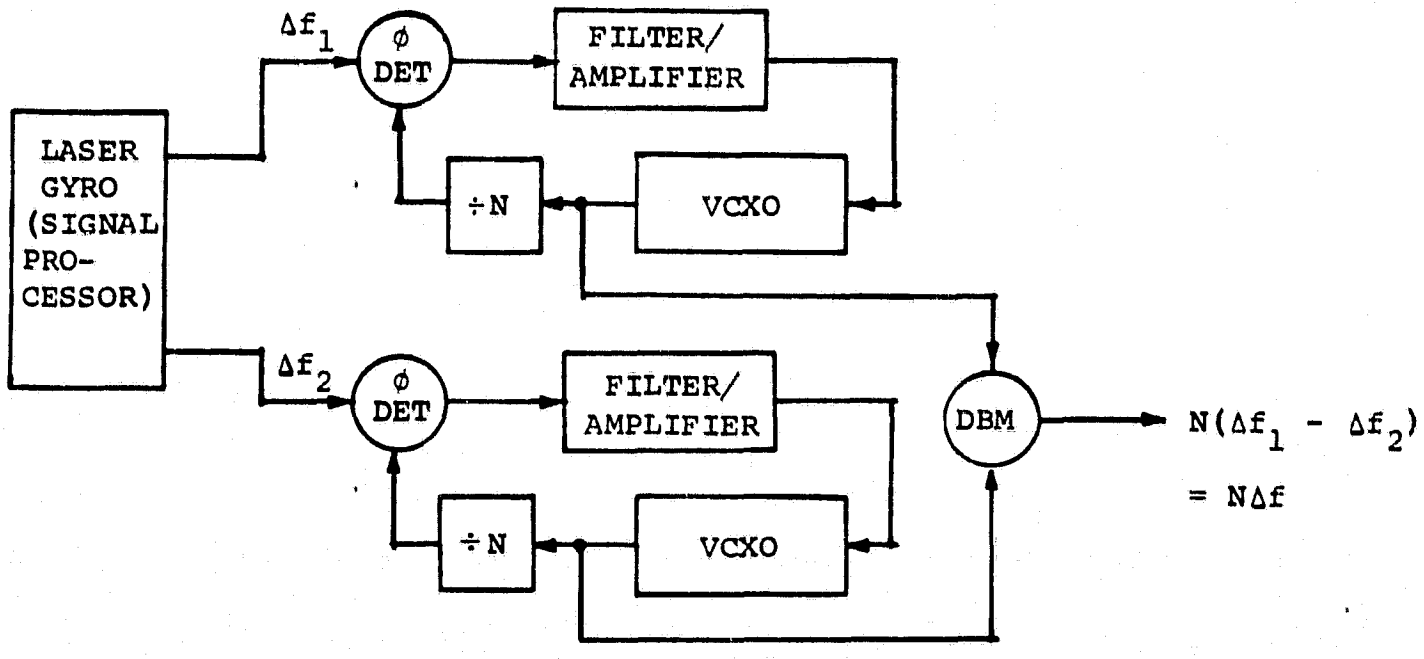

Figure 3-8 Test Circuit Block Diagram Using Double-Balanced Mixer for Output Detection

The basic circuit of Figure 3-1 can be included in the circuit of Figure 3-8 by switching in a fixed clock and an active Faraday bias coil. The added capability of this circuit provides the availability of another data point during system test.

A block diagram of the circuit selected for the final design is shown in Figure 4-1. It should be noted that this circuit is a combination of Figures 3-6 and 3-8. A dpdt switch permits the operator to select the circuit type to be used. The use of the active Faraday bias approach was included as a means to provide a second data point during system test, allowing for maximum flexibility of circuit type with a minimum of additional circuitry.

SECTION 4

FINAL ELECTRICAL DESIGN

The final design was firmed up around the block diagram of Figure 3-8. The final design is shown in Figure 4-1.

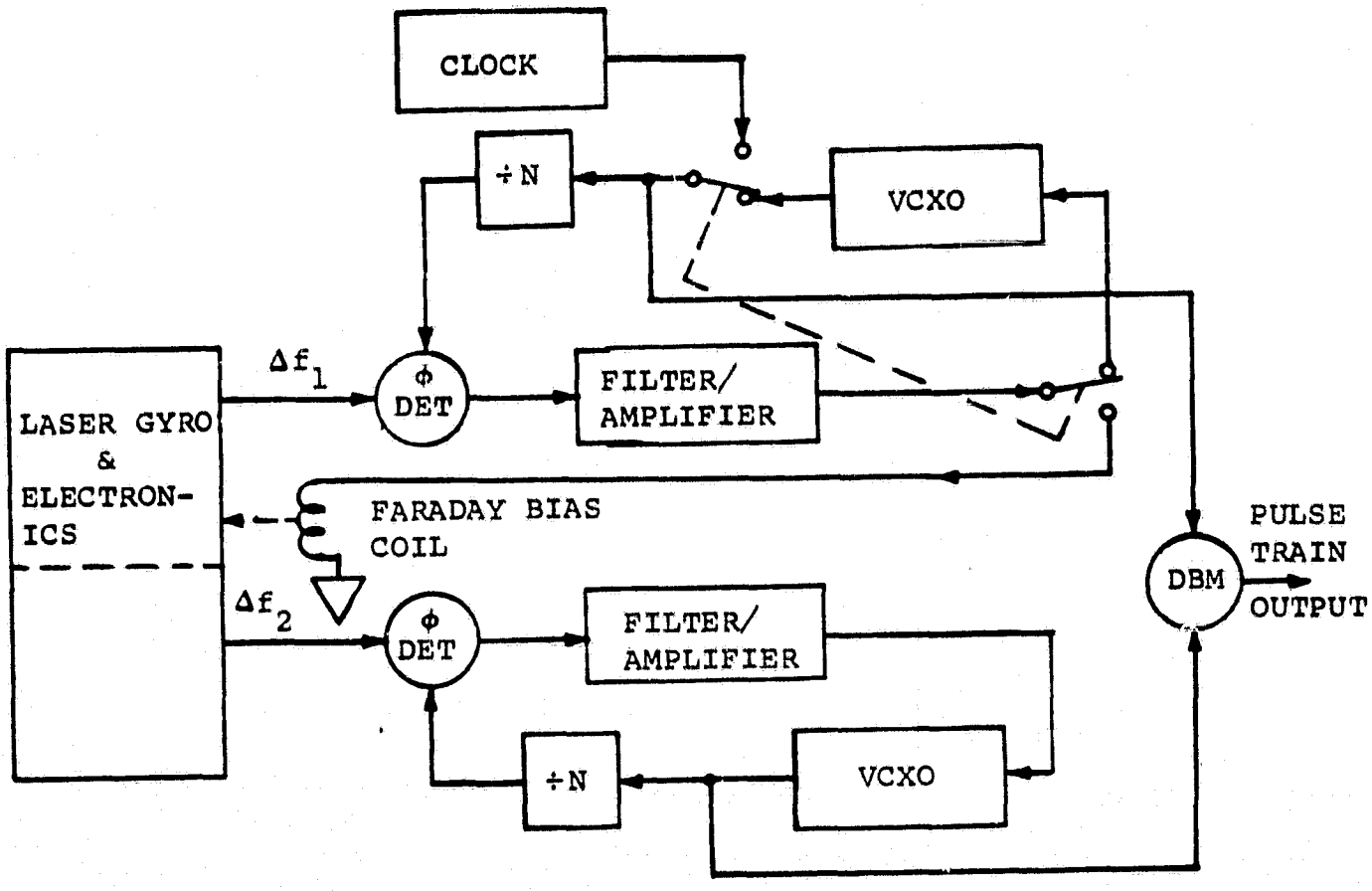

Figure 4-1 High Resolution Circuitry Block Diagram

4.1 SYSTEM OPERATION

The circuitry described in this section is dependent on Raytheon's pre-existent four-frequency ring laser gyro for its operation. The four-frequency gyro output consists of two difference frequencies, Δf_1 and Δf_2, which are produced as the discharge oscillates at four different frequencies.

These oscillations occur in traveling waves of two mutually orthogonal polarizations, one frequency at each polarization traveling around the ring in a clockwise direction, and one of each traveling in a counterclockwise direction. With the appropriate read-out system a signal can be obtained from this four-frequency gyroscope, the frequency of which is proportional to rotation rate. The read-out system consists of optics which produce two laser beams containing the two difference frequencies generated by the Faraday rotator located in the ring. These two beams contain frequency components in two ranges. The low frequency component is used to maintain a balanced amplitude in the high frequency component. The high frequency component in each beam consists of the difference frequency of the clockwise and counterclockwise beams of either the left-hand or right-hand circular polarizations. (See Figure 4-2 for clarification). The difference frequencies are defined as $\Delta f_1 = f_2 - f_1$ and $\Delta f_2 = f_4 - f_3$. These signals are amplified and become the inputs to the high resolution circuitry.

4.2 FUNCTIONAL BLOCK DIAGRAM

A functional block diagram of the high resolution system is shown in Figure 4-3. The system is subdivided into four sections, each defining a particular subsystem function. These subsystems

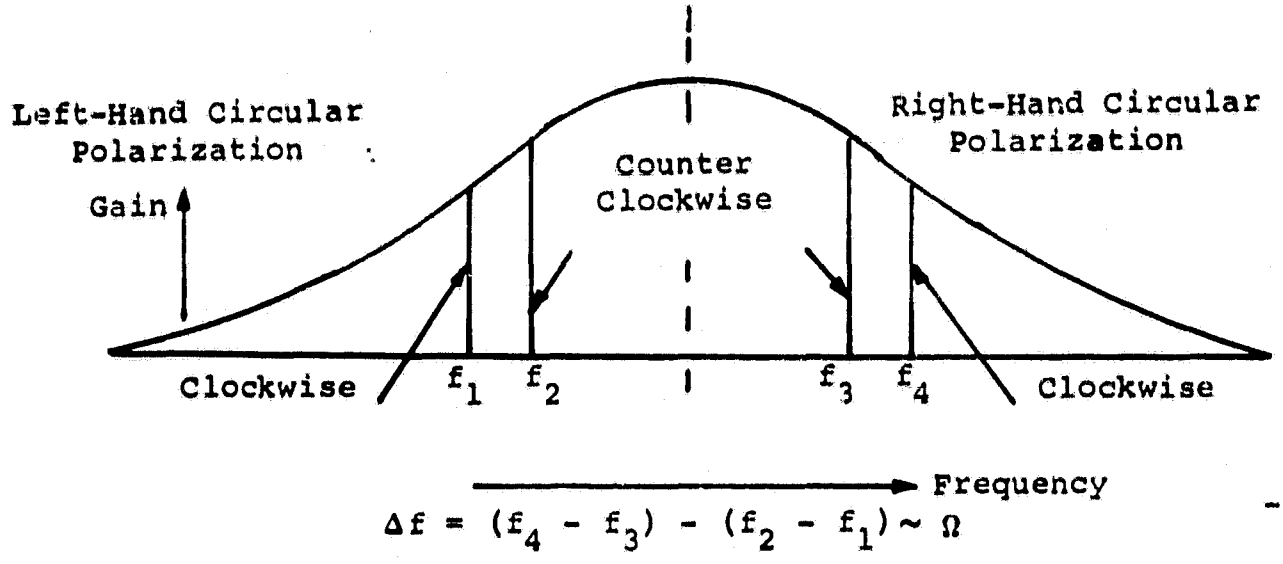

Figure 4-2 Gain Curve of Four-Frequency Gyro

are: the reference clock, the Δf_1 phase locked loop, and Δf_2 phase locked loop, and the frequency differencing network. There are three phase locked loops in the system, only two of which are fully powered at a time. The reference clock, used in conjunction with the Faraday coil, is locked to an external one-megahertz standard during its operation. Since such a standard is readily available and frequency standards in the desired range (70 MHz) would be a special design, this approach to a clock standard was used to add flexibility into the system. The reference clock is enabled by switch S2. This switch applies power to the clock loop while removing power from the VCO in the Δf_1 PLL and also removes the short circuit from the Faraday coil. The Faraday bias frequency, Δf_1, now becomes the VCO in the Δf_1 PLL, locking it to the reference clock output after dividing the clock

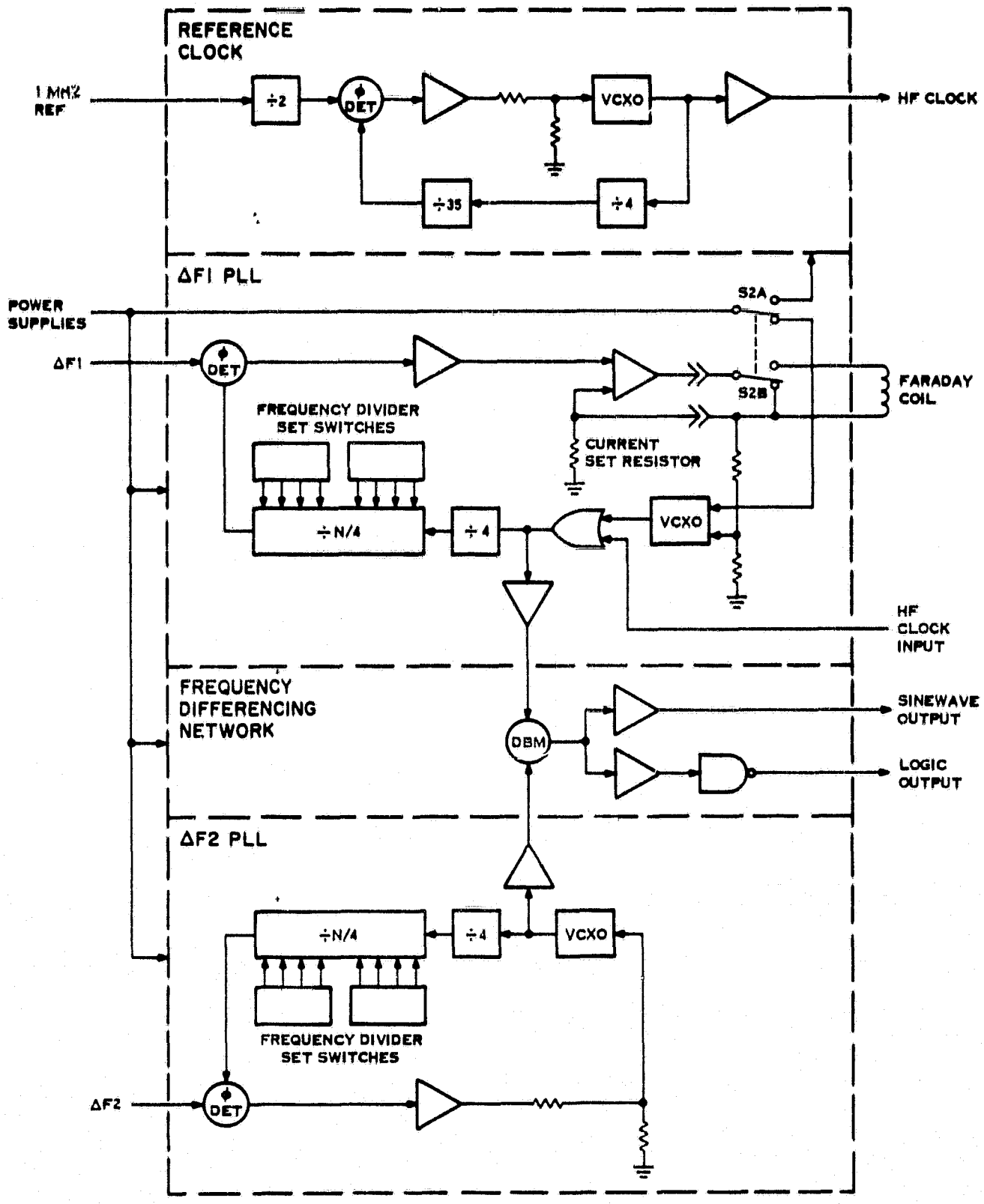

Figure 4-3 Functional Block Diagram of the High Resolution Circuit (Previously reduced to practice)

by "N". The reference clock is also routed to the frequency differencing network where it is mixed with the output from Δf_2 PLL in a double balanced mixer (DBM). The difference frequency is filtered out and amplified.

In the S2 switch position shown, the Faraday coil is disabled and the VCO's of the Δf_1 PLL and the Δf_2 PLL are locked to the Faraday bias frequencies through frequency dividers. The divide down ratio is determined by the equation

$$N = \frac{70 \times 10^6 \text{ Hz}}{\text{Faraday bias frequency}}$$

and is set into the programmable counter using the frequency divider set switches. (See Appendix D.)

4.3 CIRCUIT MODULES

The existence of near-equal high frequency signals demanded careful packaging techniques, particularly since the frequency sources are voltage controlled. Small signal coupling into the control line causes them to experience a lock-in tendency. To prevent this, the circuitry was subdivided into four functional subsections and fabricated in an rf-tight container. Input and output signals and power were supplied through connectors and feedthrough capacitors. The modules are constructed so as to allow them to be mounted on a standard 19-inch panel. The panel contains the ON/OFF switch and the mode switch. It also supports the wiring harness and connectors. The connectors are all identical and are keyed only by module location. Module locations are keyed by the input co-axial connector hole location through the front panel. A photograph of the entire unit is shown in Figure 4-4. The panel switch labelled S1, which does not appear in the functional block diagram controls DC power into the module.

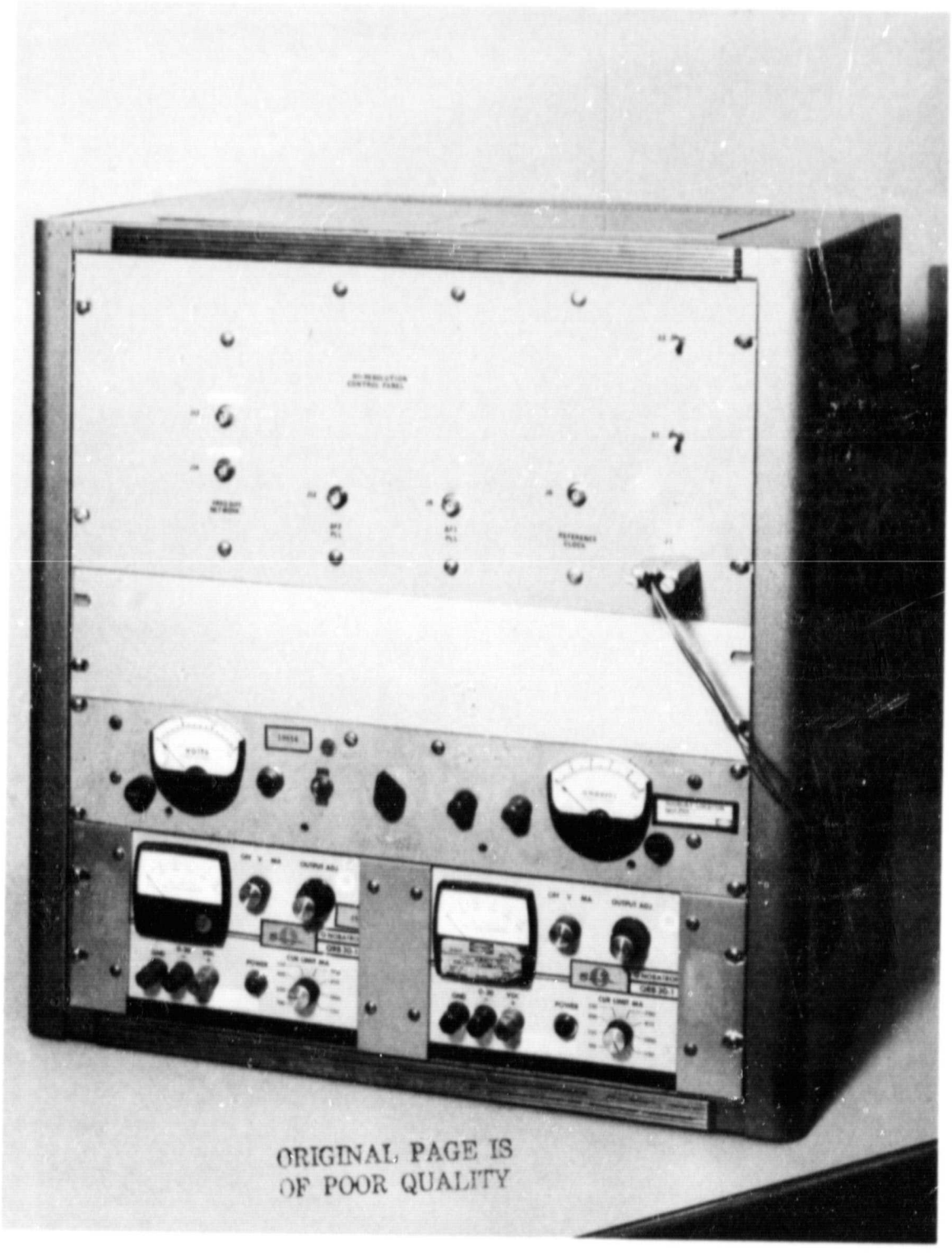

Figure 4-4 High Resolution Angular Sensor

The three phase-locked loops of the system are identical in type and order as well as in divide-down circuit construction. All are type one, first order loops. A small capacitor, located in the forward gain amplifier circuit, provides filtering for the high frequency switching edges of the digital phase detector. The three frequency dividers are constructed using two ECL data flip-flops and two high speed four-bit binary counters. The two counters are connected in series to form a maximum divide-down of 512.

4.3.1 Δf_1 PHASE LOCKED LOOP (Figure 4-5)

The Δf_1 PLL circuit requires a single input signal to function. This signal, labeled Δf_1 on the front panel, can be either a pulse train or sinusoid of two volts peak-to-peak minimum. The frequency of this signal must fall in the range of one of the frequencies shown in the table in Appendix D.

Signal frequency range is determined by the equation

$$\Delta f_1 = \frac{70 \times 10^6 \pm 2600}{4\ N}$$

where N is an integer in the range of 1 to 128, the 4 is generated by the ECL. The number, N, is programmed into the circuitry by setting two sets of four dual-inline-package (DIP) switches on the circuit board of the Δf_1 PLL module. The output of these counters is a digital pulse train which is compared with the incoming Δf_1 signal from the pulse shaping circuit. The comparison is made in a digital phase detector. The output of the phase detector is a negative going pulse from one of the two outputs, depending on the frequency phase relationship of the two input signals. These signals provide

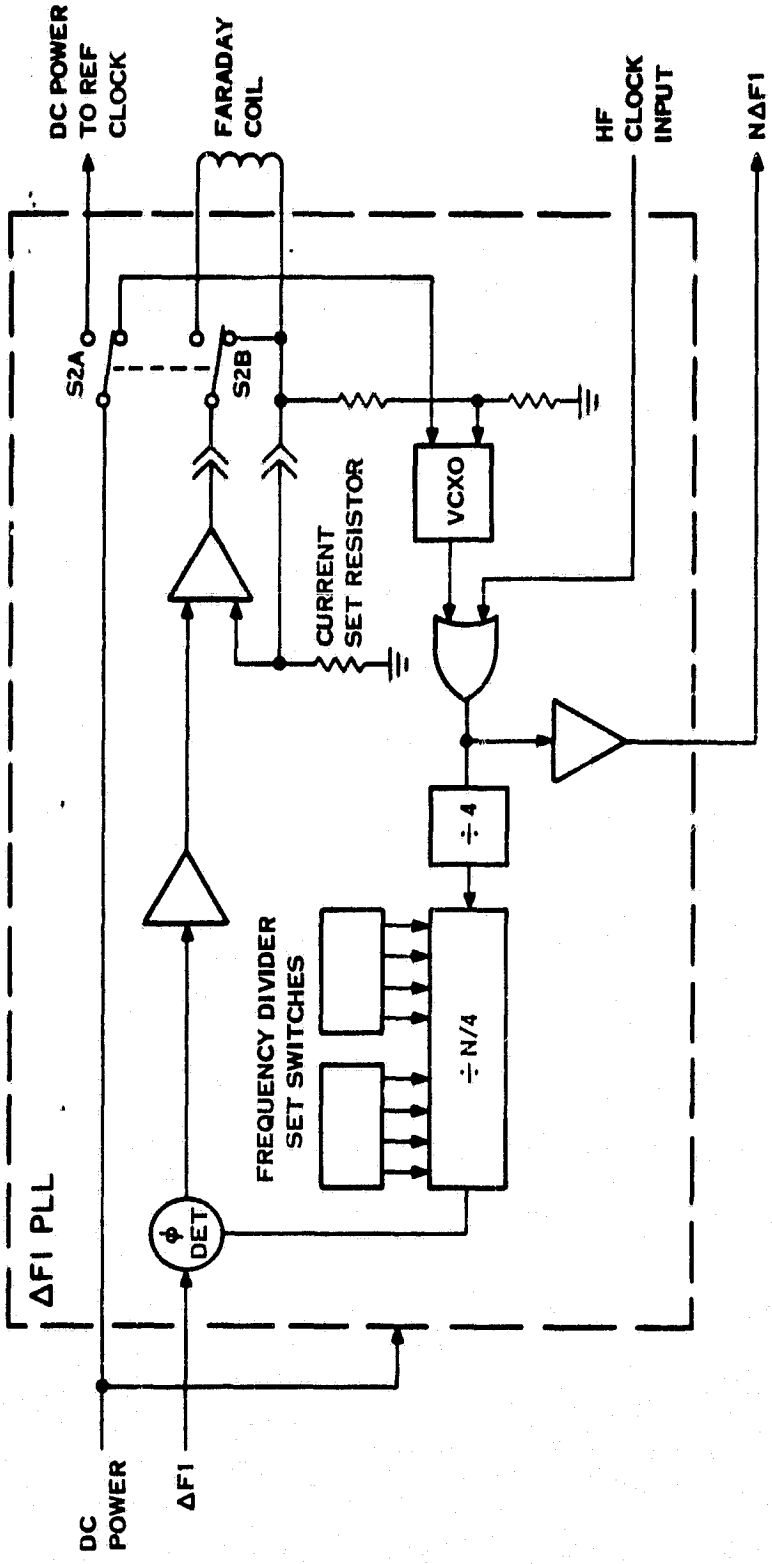

Figure 4-5 Δf_1 Phase Locked Loop Block Diagram
(Previously Reduced to Practice)

the inputs to a differential amplifier whose voltage gain of 26.8 and roll-off frequency of 23 Hz, supply the amplitude and filtering required to drive the voltage-controlled crystal oscillator (VCXO), a Motorola unit number K1085A-375-73-70 MHz. See Appendix E for a specification sheet. A second amplifier provides a voltage to current conversion for the active Faraday bias coil and functions as a voltage follower when this coil is shorted by front panel switch, S2, of Figure 4-3. The VCXO output is directed both to the PLL count-down circuit and to the frequency differencing circuitry located in a separate module. For the countdown route, an OR-ing circuit controlled by the front panel mode switch is enabled to apply the VCXO signals to a divide-by-four circuit made up of two ECL data flip flops. The 17.5 MHz output from the ECL is level shifted to drive the lower frequency TTL circuits. The VCXO output to the frequency differencing network module is also routed through a front panel controlled OR-ing network. A thin film transistor amplifier amplifies the VCXO signal and provides 50 ohm drive to the interconnecting coaxial cable.

4.3.2 Δf_2 PHASE LOCKED LOOP (Figure 4-6)

The Δf_2 PLL circuitry is similar in design and operation to the Δf_1 PLL with two notable exceptions, both of which are related to the mode switching capability of the Δf_1 PLL unit. The OR-ing networks found in the VCXO output circuit of the Δf_1 PLL and the voltage-to-current conversion amplifier are both omitted. Beyond these exceptions, circuit operation is identical.

4.3.3 FREQUENCY DIFFERENCING NETWORK (Figure 4-7)

The Frequency Differencing Network circuit receives rf signal frequencies of about 70 MHz from the two PLL's, Δf_1 and Δf_2. These signals are applied to a double balanced mixer (DBM) and the fre-

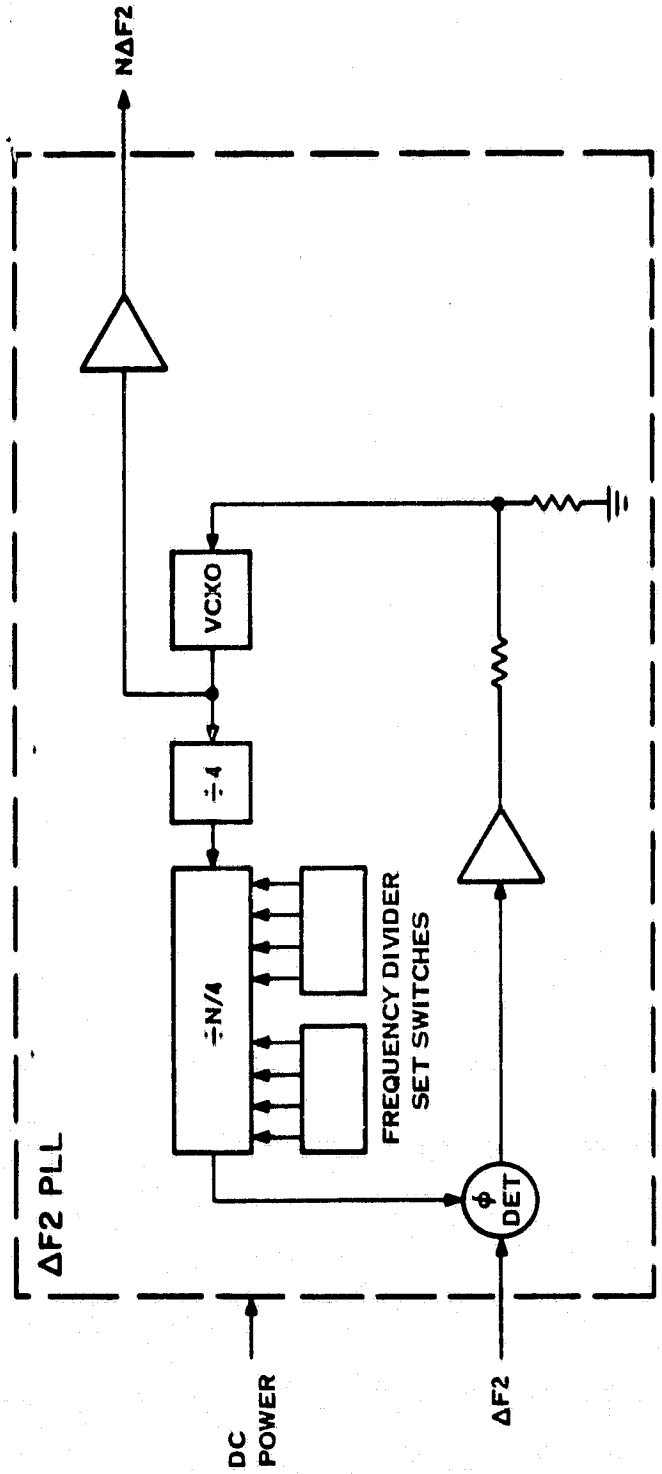

Figure 4-6 Δf_2 Phase-Locked Loop Block Diagram (Previously Reduced to Practice)

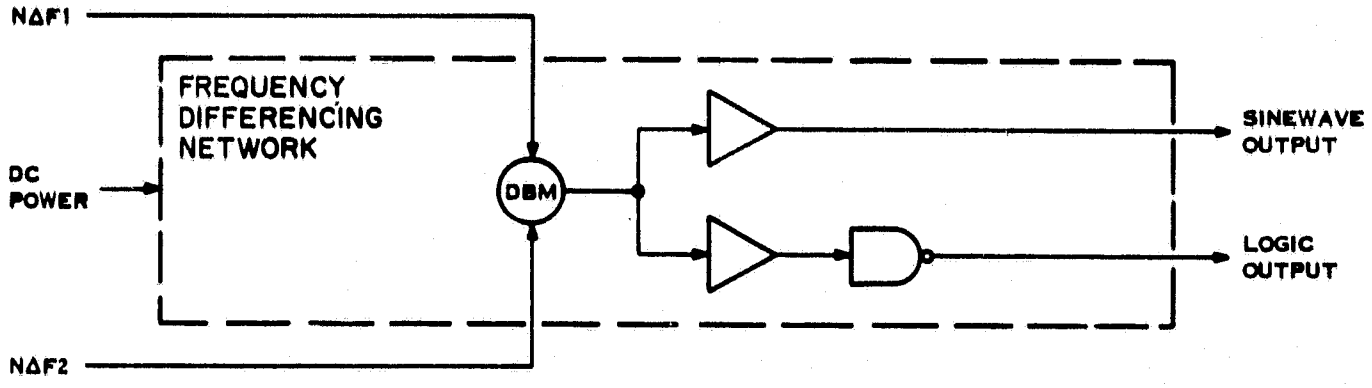

Figure 4-7 Frequency Differencing Network Block Diagram (Previously Reduced to Practice)

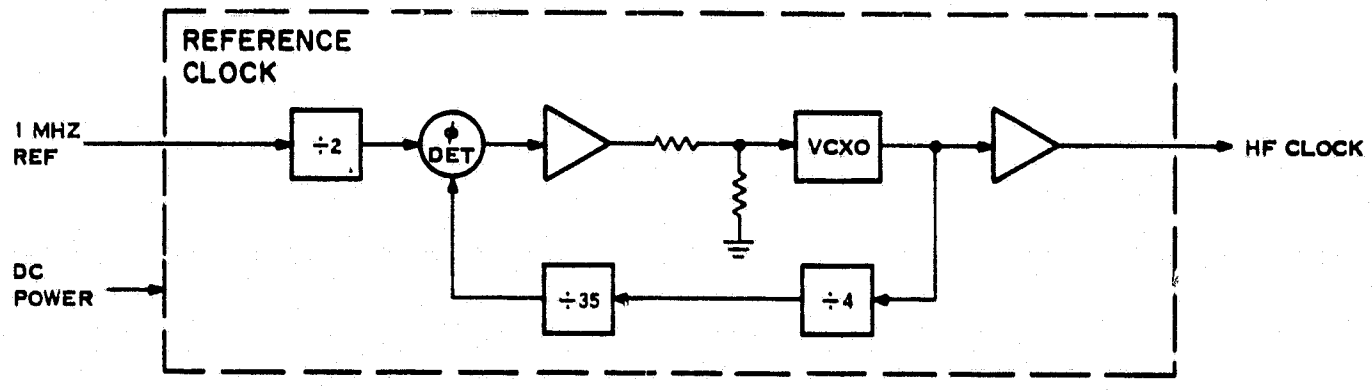

Figure 4-8 Reference Clock Phase Locked Loop Block Diagram

quency difference is selected by R-C low-pass filters. These two networks convey the signal to the two output circuit devices, a digital pulse train through a Schmitt trigger to output logic circuit; and to an analog sinewave amplifier. The outputs, both digital and analog, are available at the front panel BNC connectors.

4.3.4 REFERENCE CLOCK PHASE LOCK LOOP (Figure 4-8)

The Reference Clock PLL design is also similar to the Δf_1 PLL circuit, but with several important exceptions. These exceptions are the result of the function performed by this unit. A pulse shaping circuit converts the incoming 1 MHz reference signal to a digital pulse train to drive the divide-by-2 circuit. The phase detector compares the incoming reference, now at 500 KHz, with the frequency and phase of the counted-down VCXO output and produces a correction pulse train of proper polarity and duty cycle. This pulse train is amplified and filtered by a differential amplifier and the resulting dc voltage is applied to the VCXO control line. The VCXO, a Motorola type K1085A-331-72-70 MHz, produces a 70 MHz sine wave which is divided by 140 in a hard-wired circuit for comparison with the reference. An isolation amplifier isolates and amplifies the VCXO output for transmission to the Δf_1 PLL OR-ing circuit. The photograph in Figure 4-9 shows this module and its circuit layout alongside the panel containing the remaining modules. This module is attached to the panel by the tapped holes in the extensions of the surface on which the BNC connector is located.

4.4 AUXILIARY CIRCUITS

The wide variations in Faraday bias (and Zeeman splitting) frequencies of the laser gyroscope employed in testing the high resolution circuitry made the selection of special purchase VCXO's impractical.

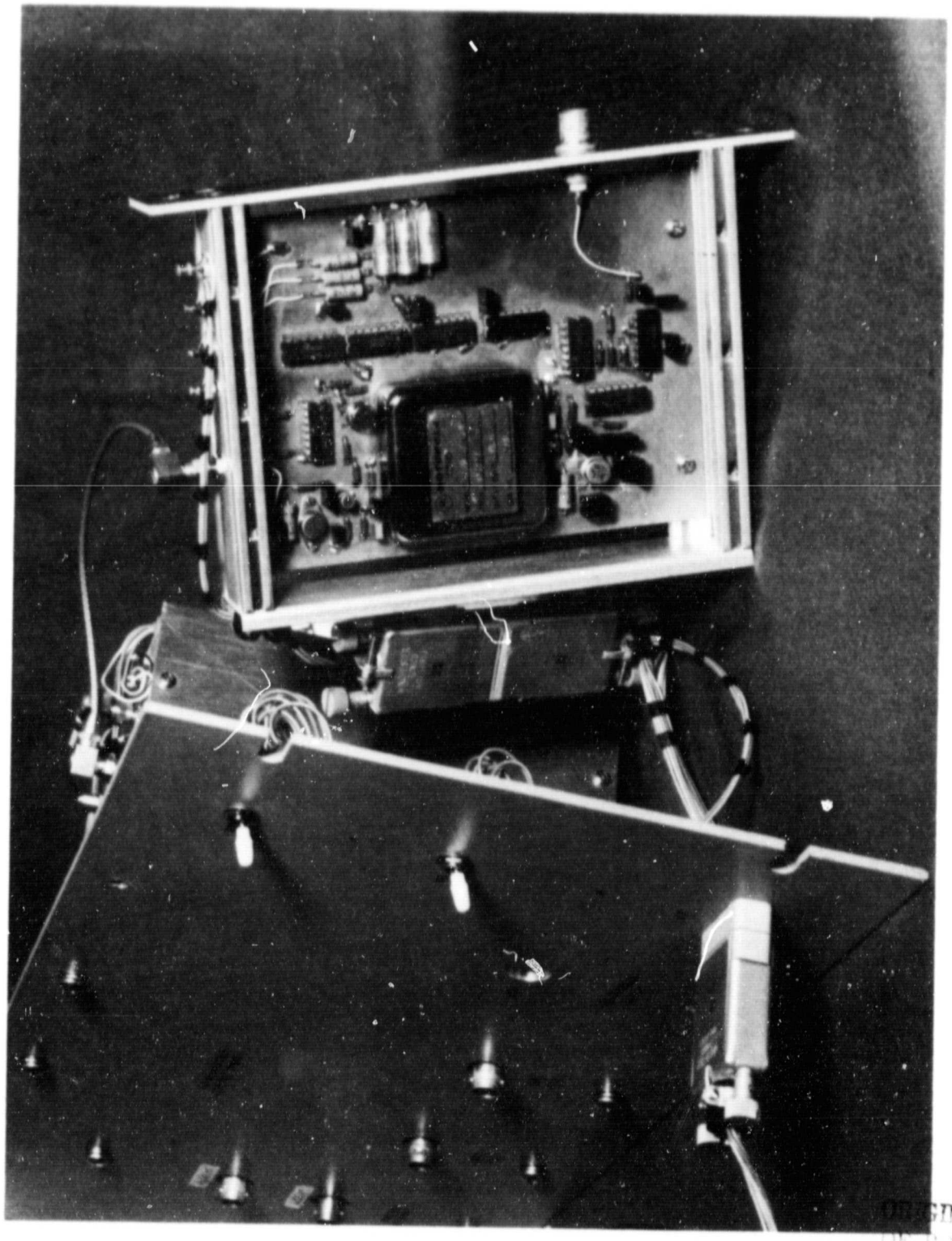

Figure 4-9 High Resolution Angular Sensor Reference Clock Module

The VCXO's used in the design are a single design type and, though tunable over a small frequency range, are not capable of accepting the input frequency variations required. Consequently, a method to overcome this laboratory environment testing problem was devised. A block diagram of the solution is shown in Figure 4-10. The function of the circuit is to shift the frequency of each VCXO by a controllable amount to accommodate values of Δf where

$$\Delta f = \Delta f_1 - \Delta f_2 .$$

The two synthesizer outputs are derived from the same clock so they add no measurable frequency jitter to the system. A bandpass filter selects the difference frequency from the DBM. This filter is discussed further in paragraph 4.5. A Hewlett-Packard 5100B synthesizer was the selected source for this test circuit because of its frequency resolution capability (to 0.01 Hz). However, the output reference frequency of the synthesizer is only 1 MHz. Consequently, a second circuit was necessary to multiply the 1 MHz reference to coincide with the requirements of the bandpass filter. Selecting 1 MHz at 70 MHz was considered to be the more difficult approach. A block diagram of the frequency multiplier is shown in Figure 4-11.

4.5 CIRCUIT TESTING AND INTEGRATION

Circuit testing was performed in four phases: (1) unit or module test; (2) testing of auxiliary circuits and circuit components; (3) system integration and bench testing as a system; and (4) system integration and testing with laser gyros. These will be discussed in order in the following paragraphs.

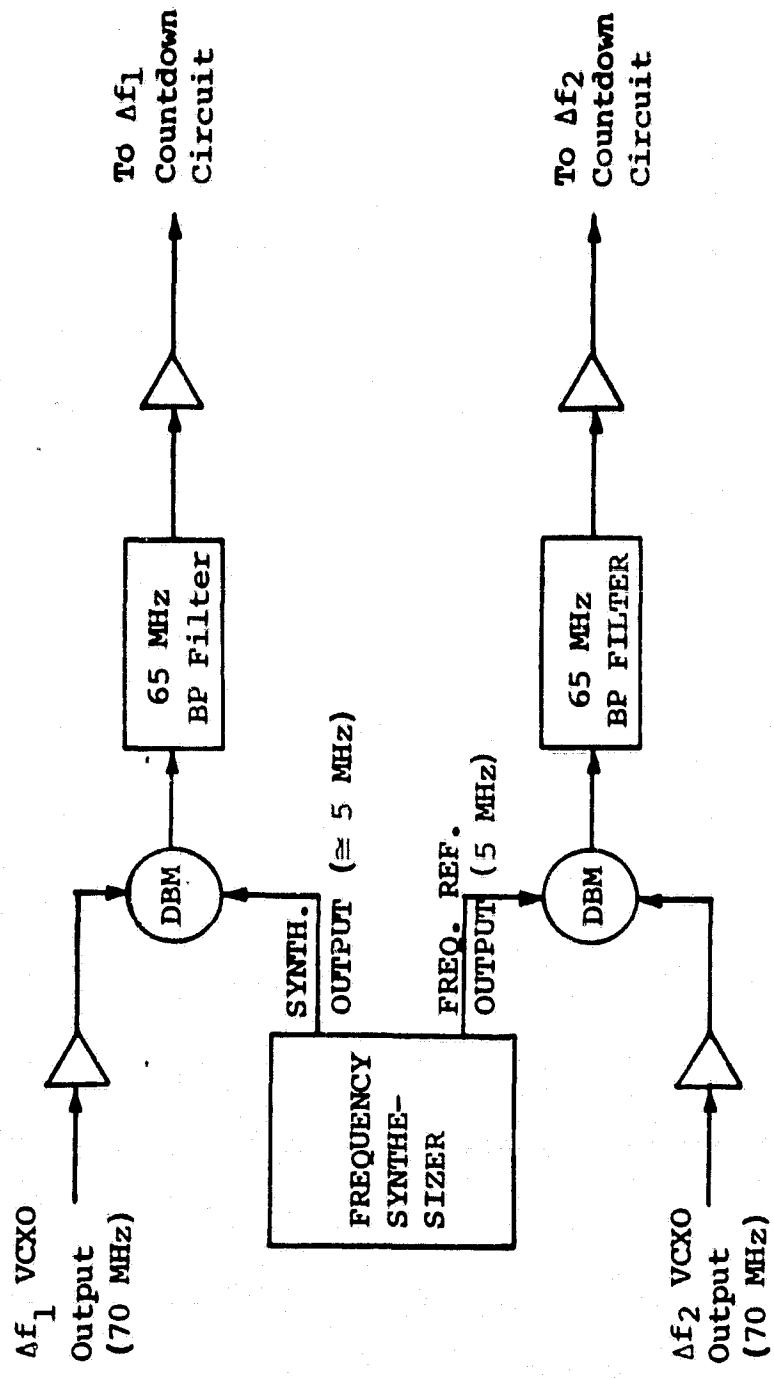

Figure 4-10 Block Diagram of Frequency Shift Approach for Laboratory Testing of High Resolution Circuitry (Previously Reduced to Practice)

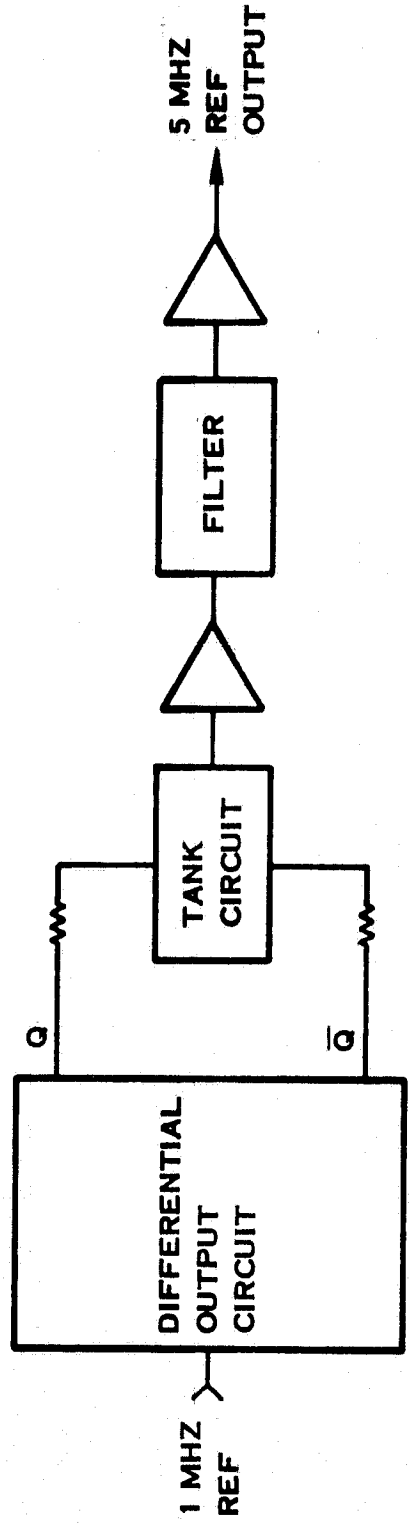

Figure 4-11 Frequency Multiplier (X5) Block Diagram
(Previously Reduced to Practice)

4.5.1 UNIT TESTS

Using a frequency synthesizer as a signal source, each of the PLL's were tested for lock and lock range. The setability of the countdown circuits was also tested over a limited range.

4.5.2 AUXILIARY CIRCUIT AND COMPONENT TESTING

The design of the frequency shift network of Figure 4-10 is contingent on the selectivity of 65 MHz bandpass filters. An in-house computer-aided filter design program was used to determine filter construction and circuit values. A copy of the programming instructions, the resulting circuitry values and the projected filter response is included in Appendix F. These filters were constructed and tested. Photos of filter response are found in Figure 4-12.

4.5.3 SYSTEM BENCH TESTING

System bench testing was carried out in two phases: the first test was performed using the system shown in Figure 4-1; the second test incorporated the frequency multiplier and the frequency shift circuitry. The testing arrangement for each of these test sequences is shown in Figures 4-13 and 4-14. During this test phase, the frequency response and sensitivity of the frequency differencing network was tested and system stability data was taken, see Section 5.

4.5.4 FUNCTIONAL SYSTEM TESTING WITH LASER GYRO

System tests using the laser gyro began by applying an external magnetic field to the gyro discharge to move the Faraday bias frequencies to a value which the system could accept. Two sources of magnetic field were used. A permanent magnet was used to make the coarse adjustment required, then an electromagnet, powered by an adjustable

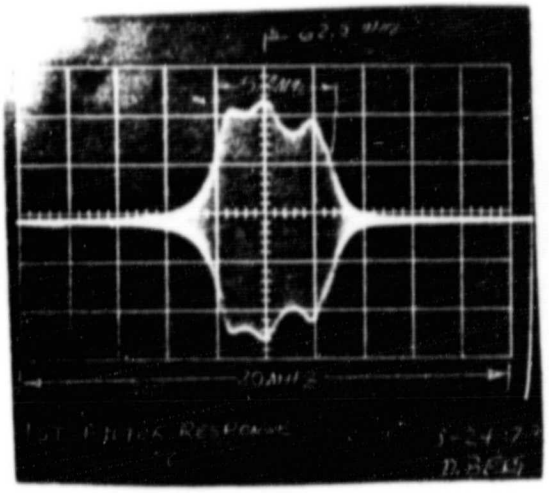

A. Envelope Response of Filter 1. Center Frequency = 63.4 MHz

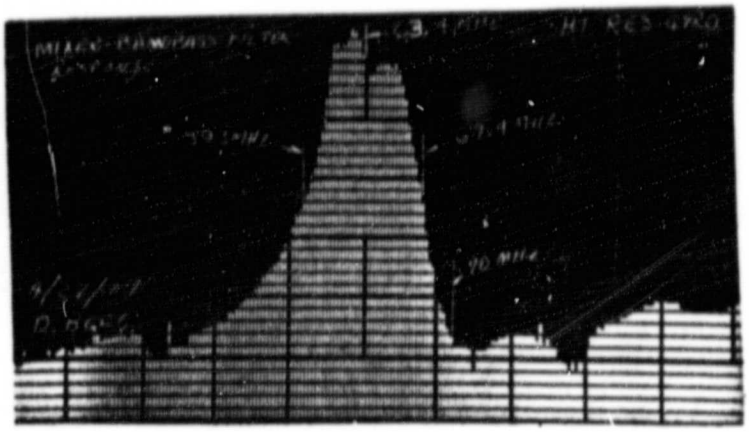

B. Detected Response of Filter 1

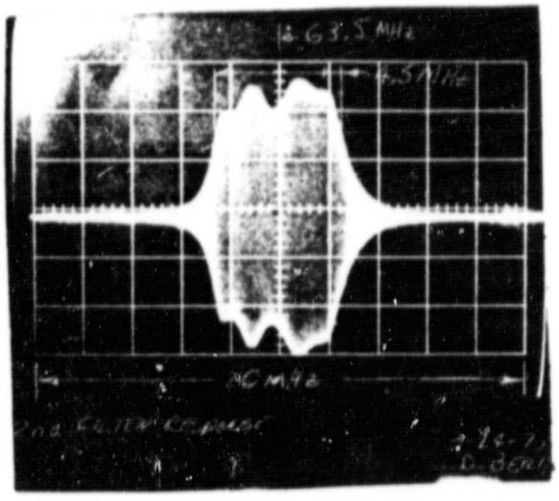

C. Envelope Response of Filter 2. Center Frequency = 63.5 MHz

Figure 4-12 Bandpass Filter Response Photos

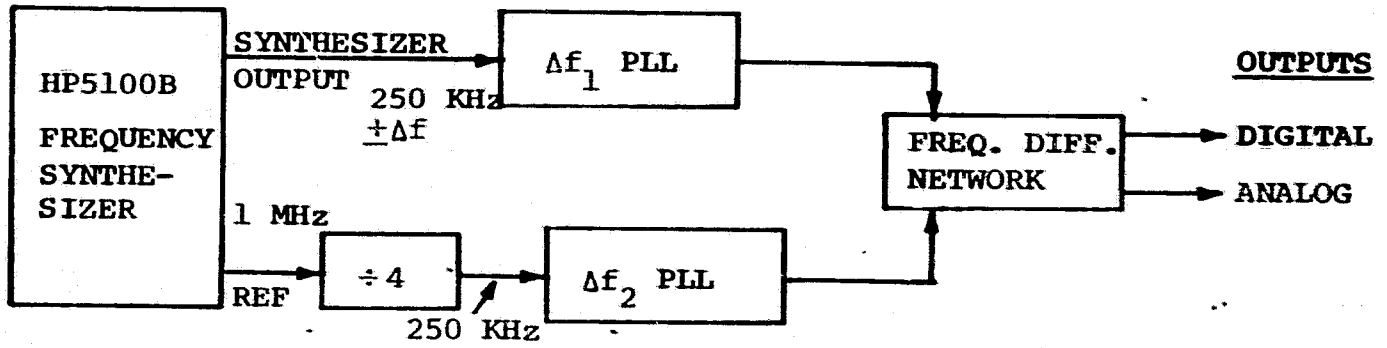

Figure 4-13 System Bench Test Arrangement

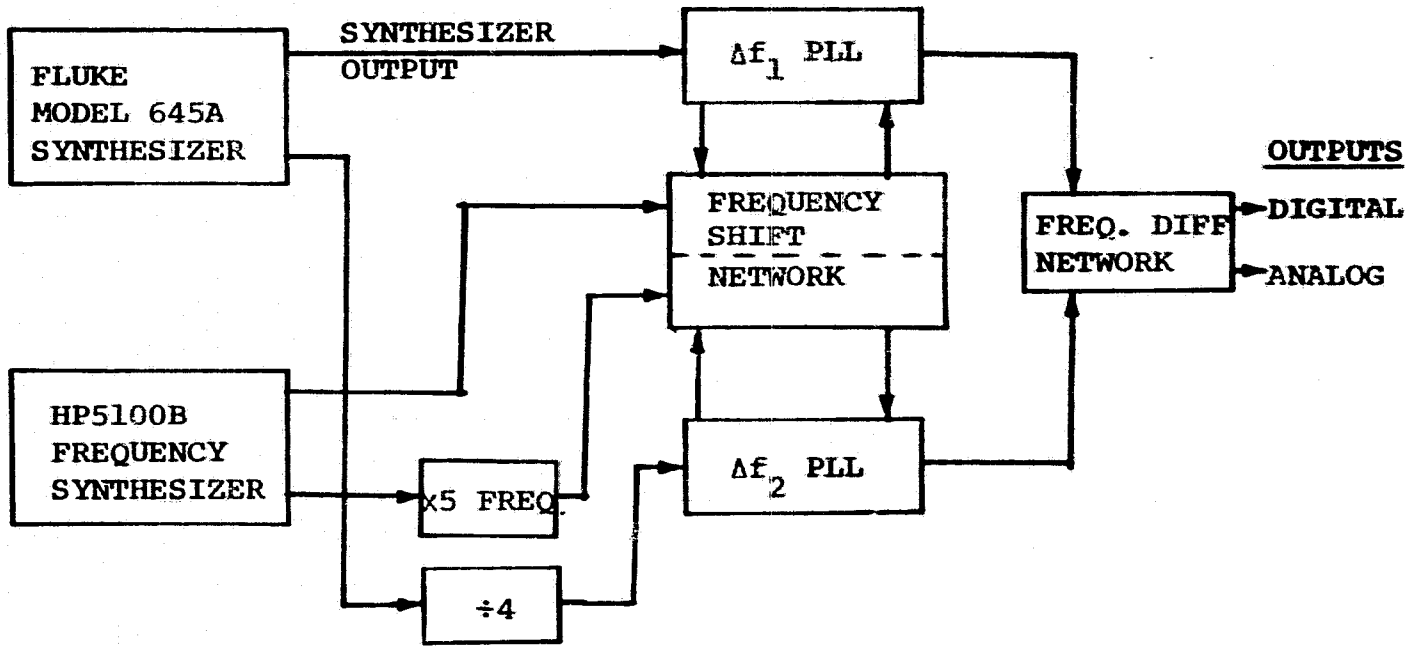

Figure 4-14 System Bench Test Using Frequency Shift Circuit and Frequency Multiplier

dc power source, was used to make the fine adjustment. Both loops were tested for lock by observing the dc feedback voltage to the VCXO. The difference frequency from the frequency differencing network was also observed and examined.

SECTION 5

SYSTEM TESTING

5.1 INTRODUCTION

Various types of system tests have been conducted using the high resolution PLL electronics. The initial testing was performed to check the noise floor of the PLL electronics and to verify that cross-talk between the dual loops was minimal. With regard to cross-talk, once the individual PLL's were checked out they were operated simultaneously and checked with a spectrum analyzer. The VCXO outputs exhibited no interference down to the noise floor of the analyzer (-60 db). The noise floor of the PLL electronics was determined by using precision frequency inputs in place of the two laser gyro inputs (Δf_1 and Δf_2). The accuracy of the PLL electronics could thus be checked by taking short term frequency stability measurements utilizing commercial test equipment.

The high resolution gyro testing was conducted in two phases. In the initial Phase I testing a Cervit block multioscillator laser gyro (designated the RB-55) was interfaced to the dual PLL electronics. The ratio of the VCXO center frequencies and the RB-55 Faraday bias frequencies allowed us to set the resolution for 0.0022 arc-seconds. In this initial demonstration test the RB-55 gyro was placed with its sensitive axis in a vertical orientation on a granite slab floating table and small azimuthal motions of the slab were excited using a small pendulum suspended below the table. In this experiment it proved possible to pick up a high resolution indication of the table motion. See Section 5.3 for the results of this initial test.

The success of the demonstration testing lead to an extension of the contract to conduct additional testing. It was the initial intent to check the gyro output at low frequency with a tiltmeter and a laser interferometer measurement system. This did not prove feasible since the tiltmeter had a lowly damped resonant mode at 0.2 Hertz and the

laser interferometer provided did not have a recording option. As previously explained in Section 1, a substitute experiment was performed in which the gyro (an RB-25 type) was mounted with its sensitive axis in the horizontal plane on a granite surface plate. A PZT similar to the one used for path length control in the gyro was used to impart small motions to the surface plate. Because the particular replacement gyro had a higher Faraday bias by a factor of 5 and a higher nominal pulse quantization by a factor of 2, a 10-fold loss in resolution capability (due to the fixed VCXO center frequency) to 0.022 arc-seconds was dictated.

This new approach to the testing of the multioscillator gyro brought forth unexpected results. We were quite surprised when the gyro detected resonances in the frequency decade beyond the nominal bandwidth (10 Hertz) of the PLL loops. These resonances are attributable to bending modes of the support structure for the granite surface plate which were excited in reaction to the PZT oscillating the plate. This higher frequency resonance was evident on the gyro output traces since it modulated lower frequency driving motions due to the PZT. As will be explained in Section 5.4, the resonant effect allowed us to detect small amplitude angular motions of the order of the resolution limit (0.022 arc-seconds) of the Phase II setup.

5.2 PLL ELECTRONICS TESTING

Tests were conducted to determine the noise floor of the PLL electronics. In these tests precision synthesized inputs were used in place of the gyro inputs. Both time domain and frequency domain data was obtained using separate equipments and the results compared.

The time domain data was taken on the HP5360A Computing Counter and the frequency domain data was taken on a recently purchased HP-5390A Frequency Stability Analyzer. The theory of measurement and the characteristics of these equipments is covered in Appendix C. For test setup convenience the resolution factor (N_R) was set for $N_R = 260$. By modifying the computing counter program slightly we

obtained the frequency deviation $\sigma_{\Delta f}$ directly instead of the fractional frequency deviation of $N_R \Delta f$. It should be remembered that Δf is the four frequency combination

$$\Delta f = \Delta f_2 - \Delta f_1 = (f_4 - f_3) - (f_2 - f_1)$$

and that one Hertz of Δf is equivalent to one arc-second/second angular rate. Thus the Computing Counter displays the equivalent rms rate error corresponding to the frequency fluctuations from the beat frequency (in this case 1040 Hertz) of the dual PLL. The data points taken on the Computing Counter are plotted on the equivalent of Figure 2-1 in Figure 5-3.

In August, 1977, the HP5390A Frequency Stability Analyzer (FSA) was used to determine the phase noise of the mixer output of the high resolution circuit. This data was then converted to an equivalent rms rate error as explained below.

The phase noise program of the FSA system is referred to as pnamh which stands for phase noise analysis modified Hadamard (refer to Appendix C for details). The signal is analyzed by way of the counter-calculator combination to provide data on the single side-band phase noise at the PLL mixer output in terms of dB/Hz versus the frequency offset (f) from the carrier in Hertz. A plot of the phase noise using nine offset frequencies (each with a measurement bandwidth of 10%) is presented in Figure 5-1.

The phase noise information [called L(f)] is convertible to phase noise power spectral density [S_ϕ (f)] in radians^2/Hertz as follows:

$$S_\phi(f) = \frac{\text{antilog } L(f)}{10}$$

A tabulation of S_ϕ (f) for the test offset frequencies is given in Table 5-1.

S_ϕ (f) may be converted very simply to the frequency fluctuation power spectral density for $N_R \Delta f$ as follows:

$$S_{N_R \Delta f}(f) = f^2 \, S_\phi(f)$$

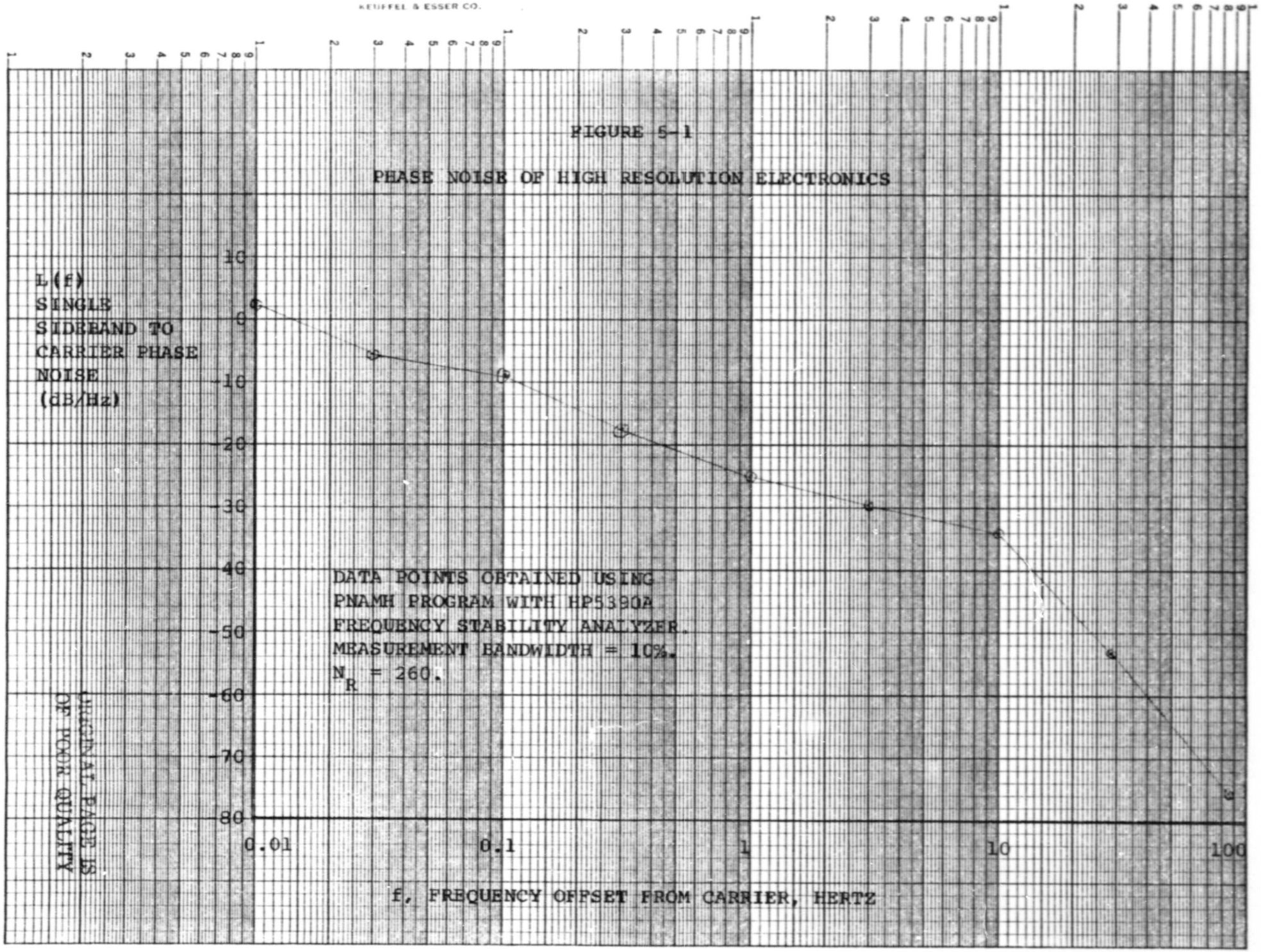

FIGURE 5-1

PHASE NOISE OF HIGH RESOLUTION ELECTRONICS

TABLE 5-1

S_ϕ (f) FOR VARIOUS OFFSET FREQUENCIES

OFFSET FREQUENCY (HERTZ)	S_ϕ (f) (RADIAN^2/HERTZ)
0.01	1.74
0.03	0.295
0.1	0.126
0.3	1.86×10^{-2}
1	3.16×10^{-3}
2.99	1.10×10^{-3}
10.19	4.07×10^{-4}
28.88	5.13×10^{-6}
86.64	2.88×10^{-8}

where $S_{N_R \Delta f}(f)$ has units of (Hertz)^2/Hertz for f, the offset frequency in Hertz and S_ϕ in (radians)^2/Hertz. Figure 5-2 presents the plot of the frequency fluctuation power spectral density.

To arrive at an equivalent time domain representation a piecewise integration, under the curve of Figure 5-2, was performed out to the experimental frequency. This gives $\sigma^2_{N_R \Delta f}$. Taking the square root and dividing by $N_R = 260$ gives $\sigma_{\Delta f}$ or σ_{rate} for Δf in Hertz and rate in arc-seconds/second. This phase noise derived data from the FSA is shown plotted on Figure 5-3 along with the direct time domain data from the Computing Counter for comparison. Very good agreement was obtained between the two methods of characterizing the noise floor of the PLL electronics and it is obvious that the measurement system noise will not interfere with high resolution gyro measurements approaching the accuracy required for such applications as the LST.

5.3 HIGH RESOLUTION DEMONSTRATION TESTING (PHASE I)

System testing with a laser gyro was undertaken once it had been determined that the noise of the PLL electronics posed no measurement interference problem. The PLL electronics were interfaced to a 55 cm path length Cervit block laser gyro (designated RB-55) previously built and tested prior to this contract. The resolution factor was set at $N_R = 364$ to be compatible with Δf_1 and Δf_2 of the gyro. This reduced the basic 0.8 arc-second quantization of the gyro to 2.2×10^{-3} arc-seconds for the high resolution digital output.

The gyro was placed on a granite slab floating table with a small pendulum suspended beneath the table (see Figure 5-4). Azimuthal motion of the table was excited by setting the pendulum in motion. The approximate period was 1.6 seconds. A special test unit (referred to as the FINC Counter) was used to sum the high resolution digital output over 0.01 second intervals and to convert the result to an analog format for strip chart recording. Figure 5-5 presents a sample re-

FIGURE 5-2

FREQUENCY MODULATION NOISE POWER
SPECTRAL DENSITY OF HIGH RESOLUTION ELECTRONICS

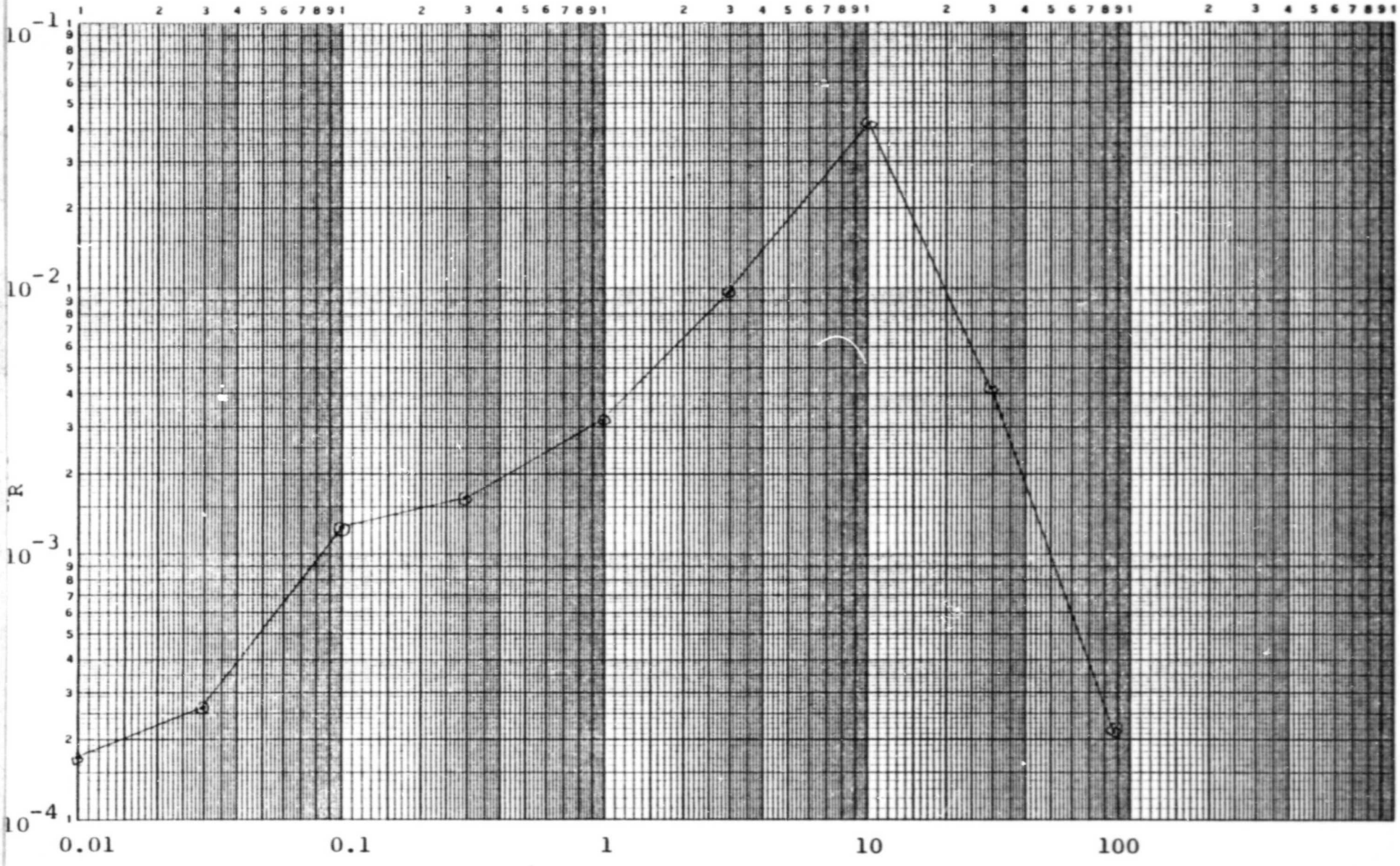

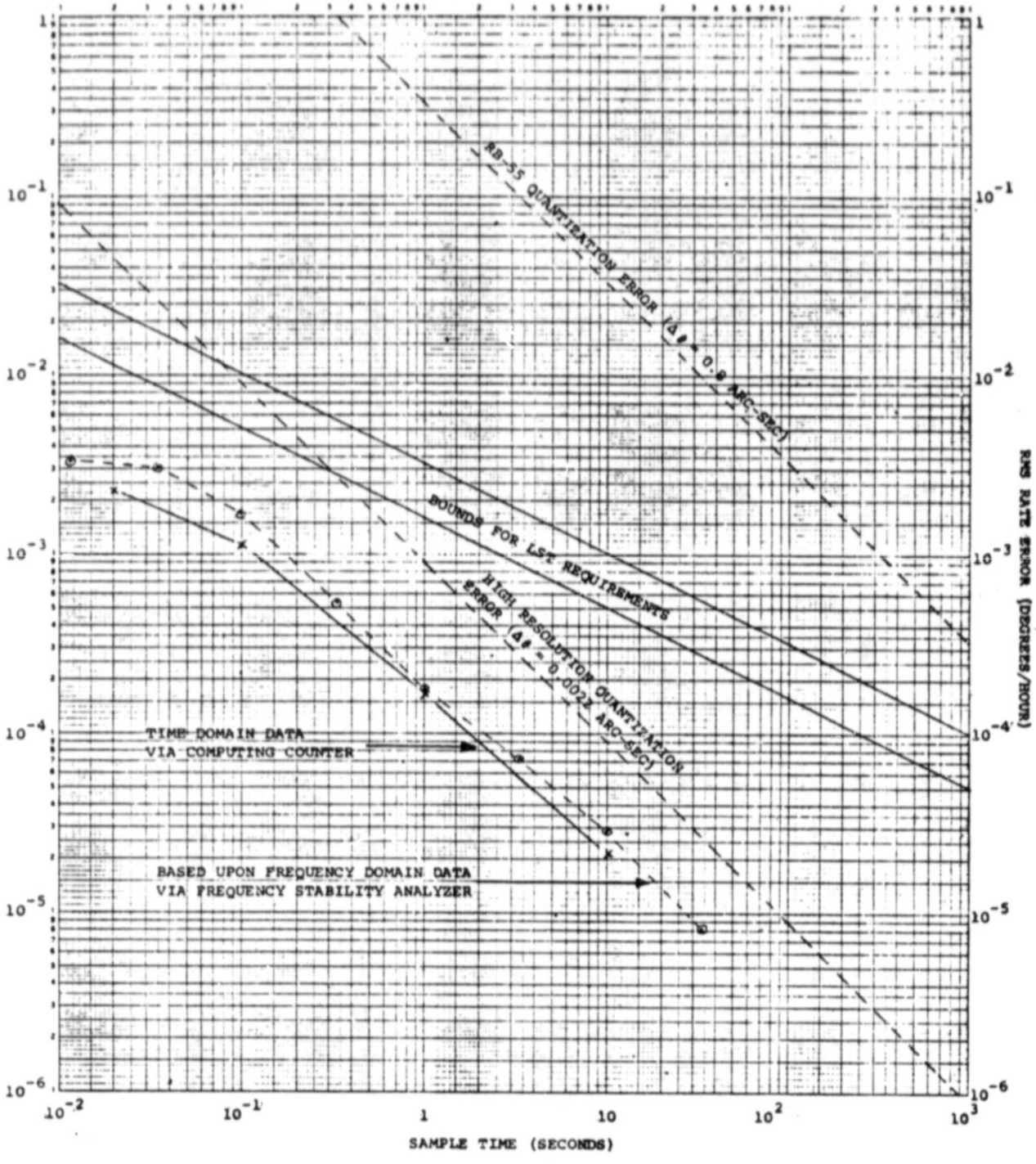

Figure 5-3. Noise Floor of PLL Electronics in Terms of Equivalent Rate Error

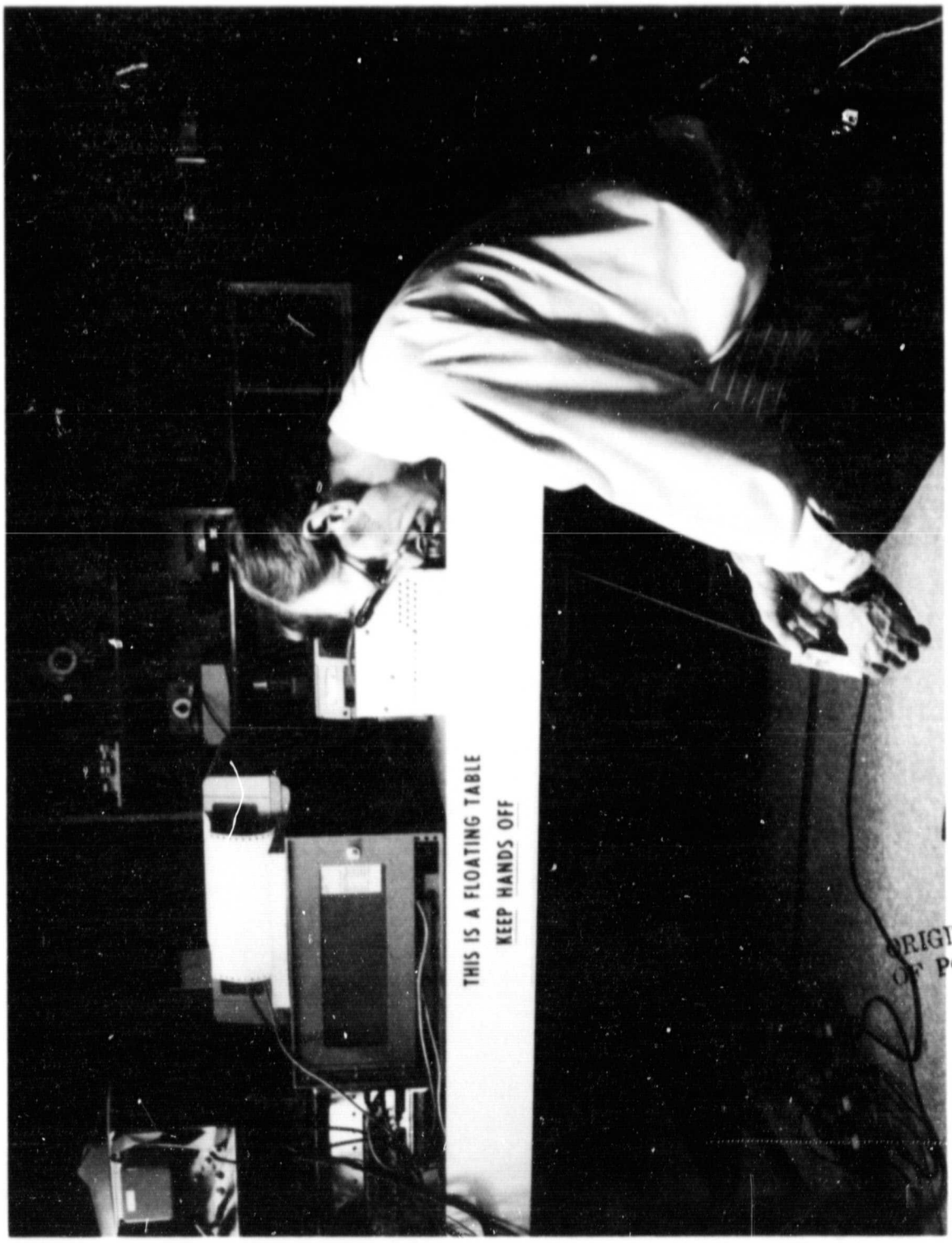

Figure 5-4. High Resolution System Testing Using a Pendulum to Excite Gyro Mounted on Floating Table

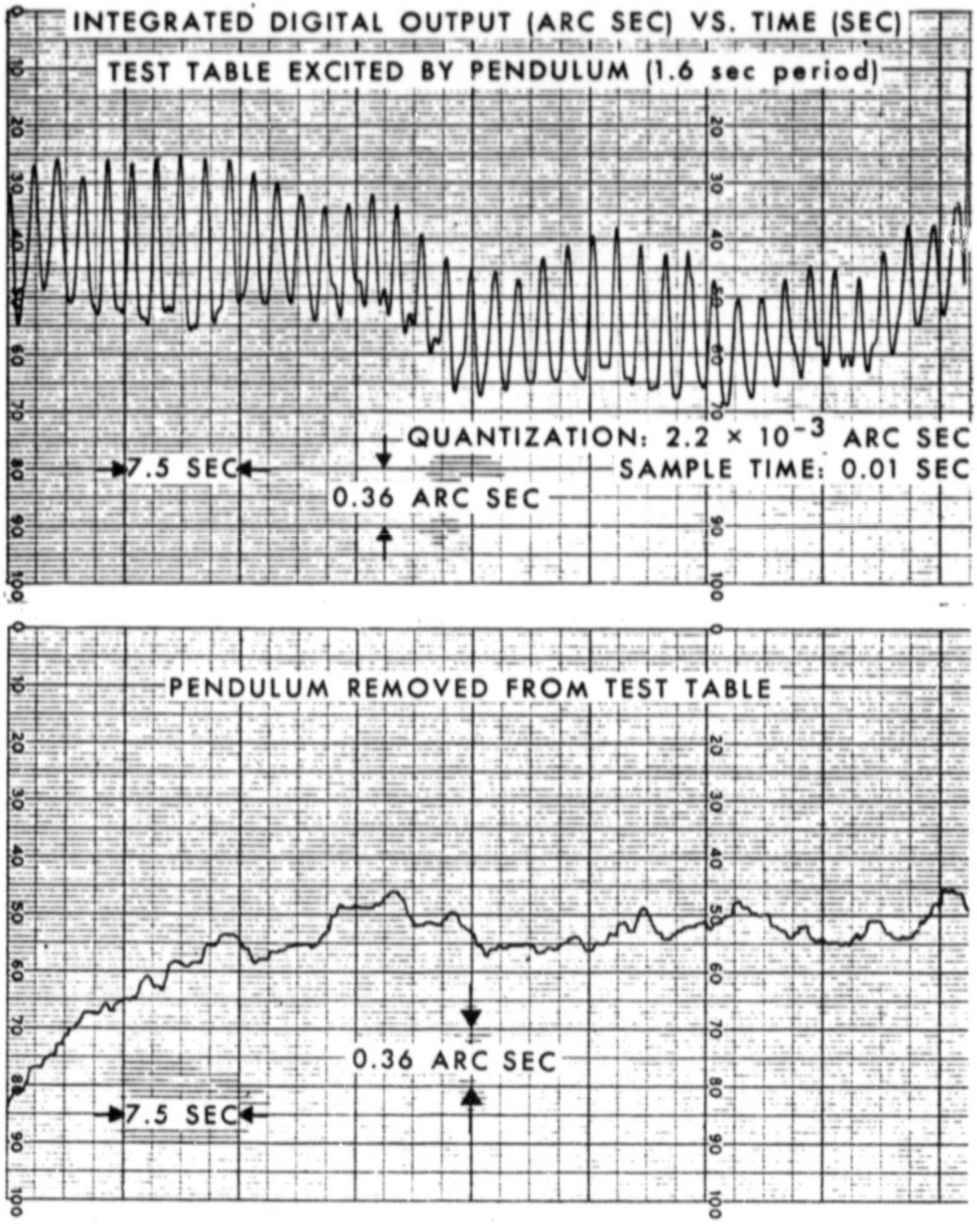

Figure 5-5. High Resolution Laser Gyro Demonstration Test Data

cording taken in this fashion. The upper trace shows the result of exciting the table by swinging the pendulum and the lower trace shows the integrated output with the pendulum at rest.

Since a spread of 20 millimeters in Figure 5-5 represents the basic 0.8 arc-second quantization of the gyro it is seen that a high resolution angular indication is being achieved. Although the actual accuracy of the gyro cannot be determined in this test it is evident from the lower trace of Figure 5-5 that changes in motion as low as 1/2 millimeter or 0.02 arc-seconds are discernible.

5.4 HIGH RESOLUTION DEMONSTRATION TESTING (PHASE II)

The RB-25-11 gyro tested in Phase II had a low frequency drift, corrected in subsequent gyros, which caused loss of lock due to the limited frequency pull range of the highly stable oscillators used in the loops. The dependence between the rms frequency deviation and pulling range of a crystal oscillator is discussed in Appendix B. By external intervention lock could be maintained for short stretchs and data obtained on the high resolution angular output of the gyro.

The strip chart trace shown in Figure 5-6 is typical of the results obtained with the PZT driving the surface plate on which the gyro was mounted with its sensitive axis in the horizontal plane. Figure 5-7 is a photograph of the setup used to oscillate the surface plate at various frequencies. The test equipment allowed the high resolution rate output of the PLL's to be digitally integrated to a angular indication and D/A sampled at a high rate for recording on a strip chart. The upper trace of Figure 5-6 is such a recording (the scale is 0.044 arc-second per mm so that each mm is equivalent to twice the resolution limit of 0.022 arc-seconds) and the lower trace is a recording of the voltage used to drive the PZT.

The data run of Figure 5-6 was made using a 10 Hertz bandwidth for the PLL's and using a PZT drive frequency of 5 Hertz. It was determined by driving the PZT at frequencies above and below 40 Hertz that the response dropped off on either side of 40 Hertz indicating a

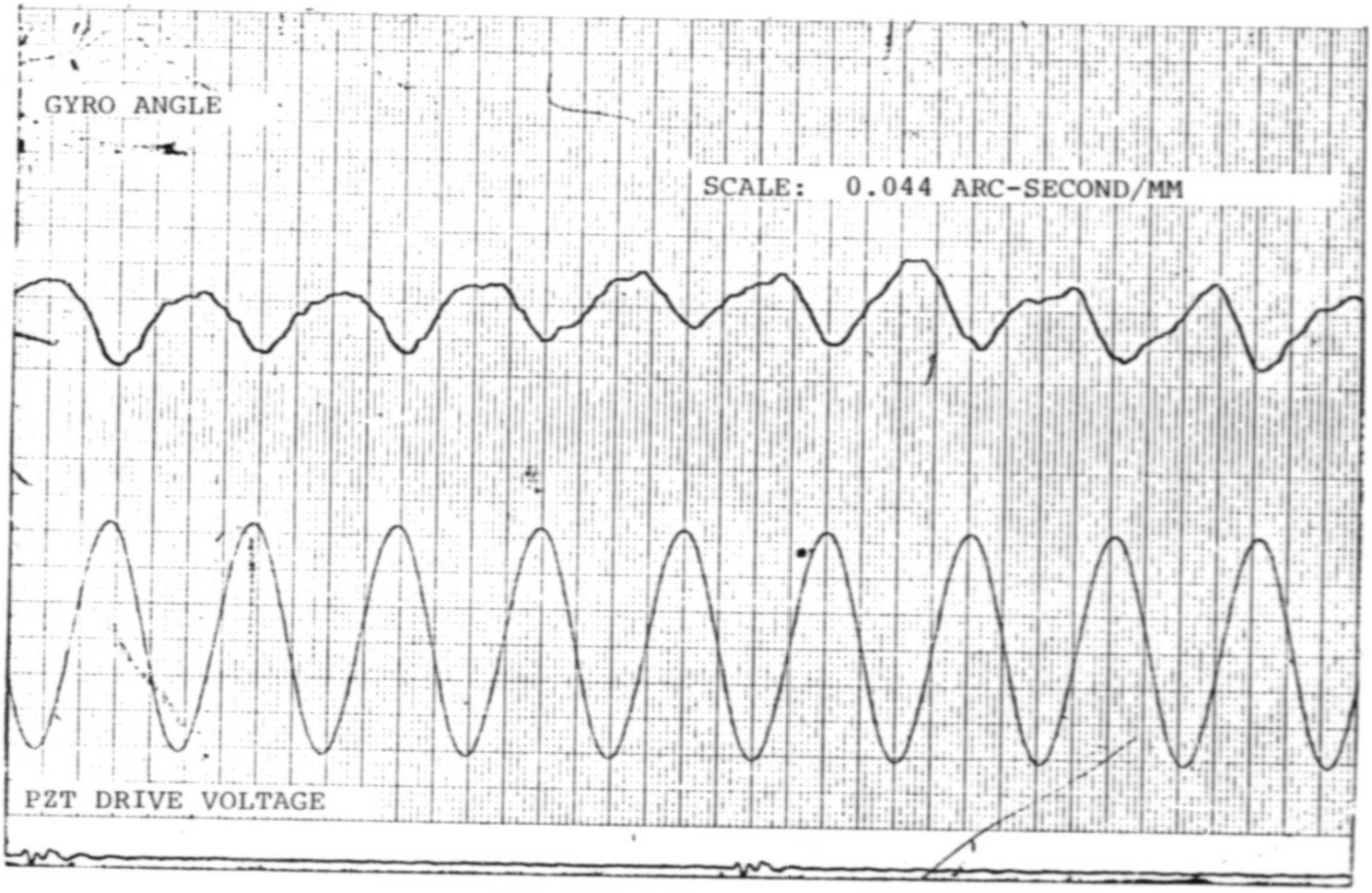

RUN CONDITIONS

Gyro sensitive axis in horizontal plane.
PZT driving surface plate.
PZT drive frequency: 5Hz.
PLL Bandwidth: 10Hz.

Figure 5-6. High Resolution Angle Output Test

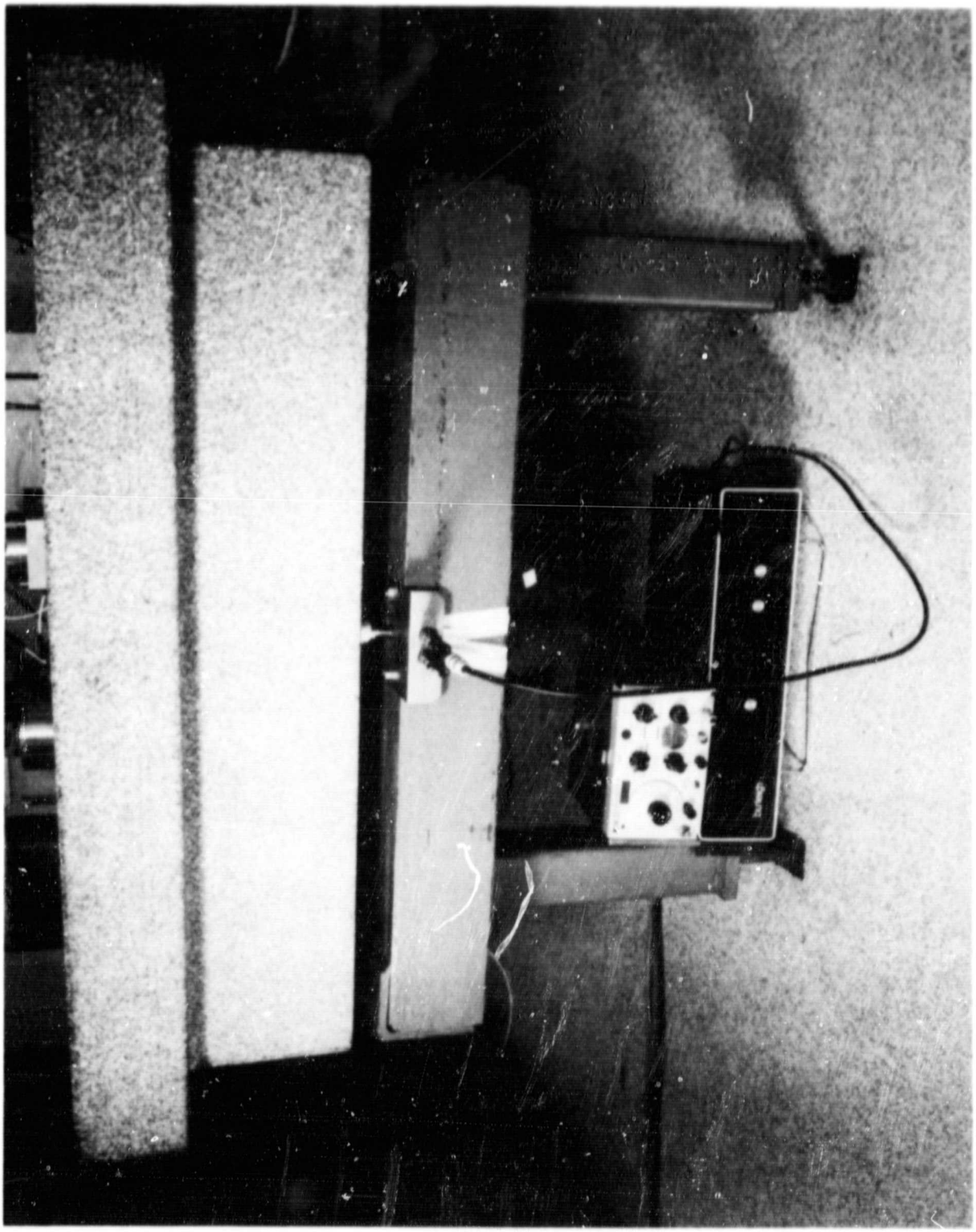

Figure 5-7. Experimental Setup for Osiclating Surface Plate

resonance at approximately that frequency. This has been attributed to a resonance in the surface plate support structure. This was experimentally verified by inserting various amounts of iso-padding between the support and the plate and observing the change in resonant frequencies. The high frequency disturbances riding on top of the basic 5 Hertz response are thus attributable to the 40 Hertz structural resonance of the surface plate support structure. Peak-to-peak variations as low as 1/2 mm are detectable which correlates with the resolution capability of 0.022 arc-seconds.

An analog indication of rate is also achievable from the circuit using a differential amplifier. To obtain gyro analog rates we put the VCXO control voltages into a differential amplifier after adjusting one of the channels to account for the relative gain variations in the two VCXO's. Figures 5-8 and 5-9 are two data runs made in this fashion. The upper traces are now analog gyro rate (scaled to 4.15 arc-seconds per second per mm). The differential amplifier apparently high-passed out the low-frequency drift of the gyro resulting in the smooth traces shown in Figures 5-8 and 5-9. In Figure 5-8 the resonance of the support structure is clearly picked up by the gyro. The average indicated rate (peak-to-peak) is approximately 25 arc-seconds per second which would translate into an equivalent peak-to-peak angle of 0.10 arc-seconds for the 40 Hertz drive frequency. Figure 5-9 is included for comparison to the run shown on Figure 5-6. The run conditions are the same for both runs. Again we see that disturbances due to the structural resonance of the surface plate support are present.

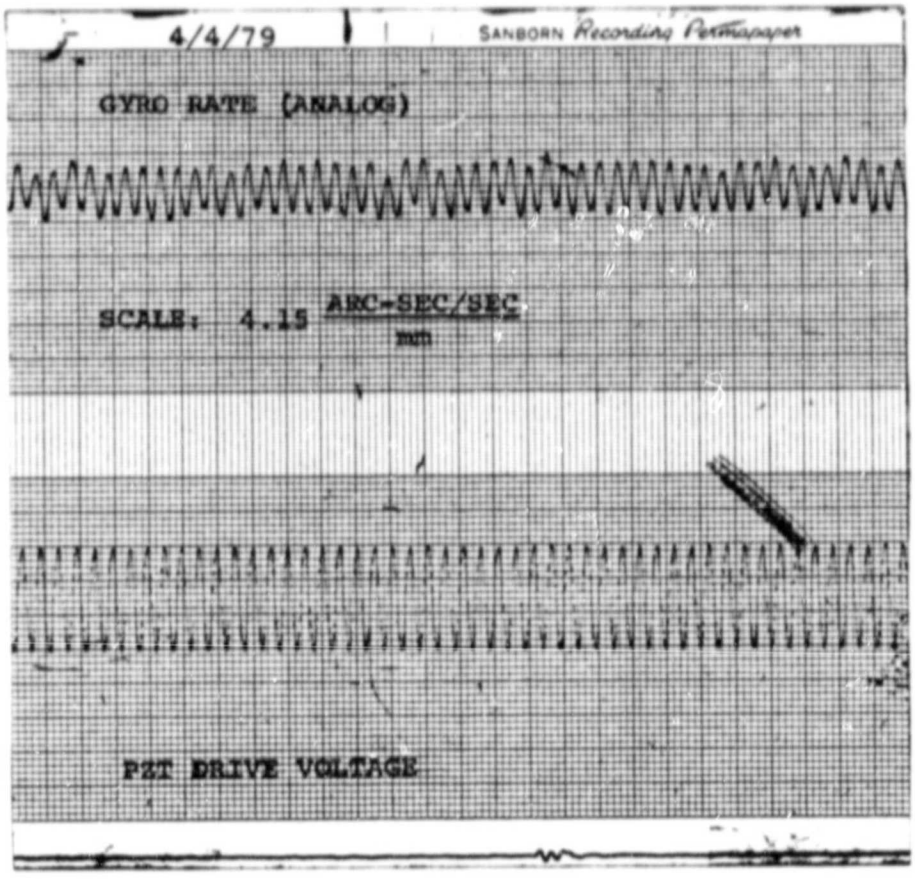

RUN CONDITIONS

GYRO SENSITIVE AXIS IN HORIZONTAL PLANE.

PZT DRIVING SURFACE PLATE.

PZT VOLTAGE: 55 VOLTS.

PZT DRIVE FREQUENCY: 40 Hz

INDICATED RATE (PEAK-TO-PEAK): 25 ARC-SEC/SEC.

EQUIVALENT ANGLE (PEAK-TO-PEAK): 0.10 ARC-SEC.

NOTE: THE GYRO IS INDICATING THE RESONANCE AT 40 Hz OF THE STRUCTURE SUPPORTINC THE GRANITE SURFACE PLATE. RESPONSE OF SURFACE PLATE DROPS OFF AS DRIVE FREQUENCY IS VARIED AWAY FROM 40 Hz.

Figure 5-8. Gyro Indication of Structural Resonance

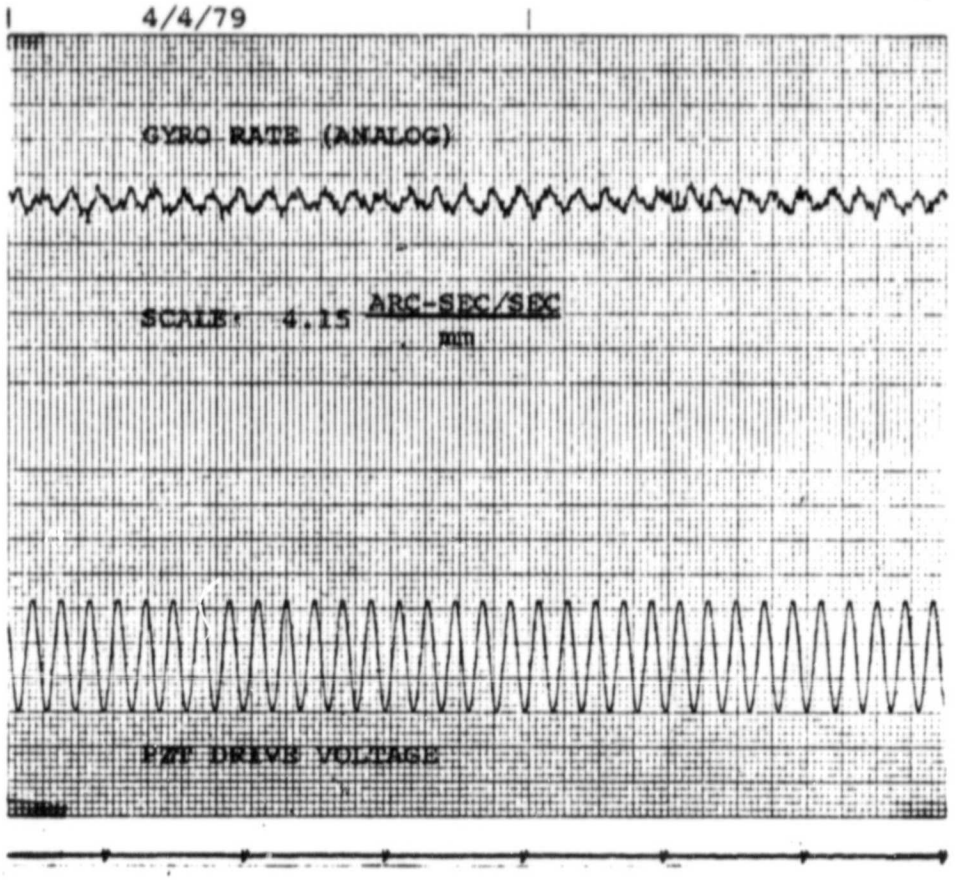

RUN CONDITIONS

GYRO SENSITIVE AXIS IN HORIZONTAL PLANE.

PZT DRIVING SURFACE PLATE.

PZT VOLTAGE: 300 VOLTS.

PZT DRIVE FREQUENCY: 5 Hz

INDICATED RATE (PEAK-TO-PEAK): 12.5 ARC-SEC/SEC.

EQUIVALENT ANGLE (PEAK-TO-PEAK): 0.4 ARC-SEC.

NOTE: THE DISTURBANCE SUPERIMPOSED UPON THE BASIC 5 Hz GYRO SIGNAL IS DUE TO THE 40 Hz STRUCTURAL RESONANCE OF THE SURFACE PLATE SUPPORT.

Figure 5-9. Gyro Response with Superimposed Structural Resonance

REFERENCES

2-1 J. R. Glaese, H. F. Kennel, G. S. Nurre, S. M. Seltzer and H. L. Shelton, "A Low Cost LST Pointing Control System", AIAA paper No. 75-1057, Presented at AIAA Guidance and Control Conference, Boston, Massachusetts, August 20 - 22, 1975.

2-2 "A High Resolution Laser Gyro Technology Development Program", Raytheon Company/Equipment Division, ER75-4438-1, 8 December 1975. Technical Proposal submitted to Marshall Space Flight Center.

2-3 A. Yariv, Introduction to Optical Electronics, Second Edition, Holt, Rinehart and Winston, 1976.

2-4 I. L. Bershtein, I. A. Andronova and Yu. I. Zaitsev, "Fluctuations in the Intensity and Frequency of a Laser" Radio Physics and Quantum Electronics, Vol. 10, No. 1, pp. 28 - 32, 1967.

2-5 G. C. Newton, L. A. Gould and J. F. Kaiser, Analytical Design of Linear Feedback Controls, John Wiley and Sons, Inc., 1957.

2-6 W. A. Edson, "Noise in Oscillators" Proceedings of the IRE, August, 1960, pp. 1454 - 1466.

3-1 M. I. Gneses and J. B. Matthews, "1975 Independent Development Program 75D-290, Laser Gyro Development Program Final Report", Raytheon Company/Equipment Division, ER75-4486, 31 December 1975.

3-2 M. I. Gneses, "1976 Independent Development Project 76D-310, Laser Gyro Advanced Technology Annual Report", Raytheon Company/Equipment Division, ER76-4429, 15 February 1977.

3-3 "1977 Independent Development Project 77D-310, Laser Gyroscope Prototype Development Annual Report", Raytheon Company/Equipment Division, to be published.

APPENDIX A

LASER GYRO QUANTIZATION ERROR

The quantization error in terms of rate may be derived by referring to Figure A-1. The simplest digital algorithm for

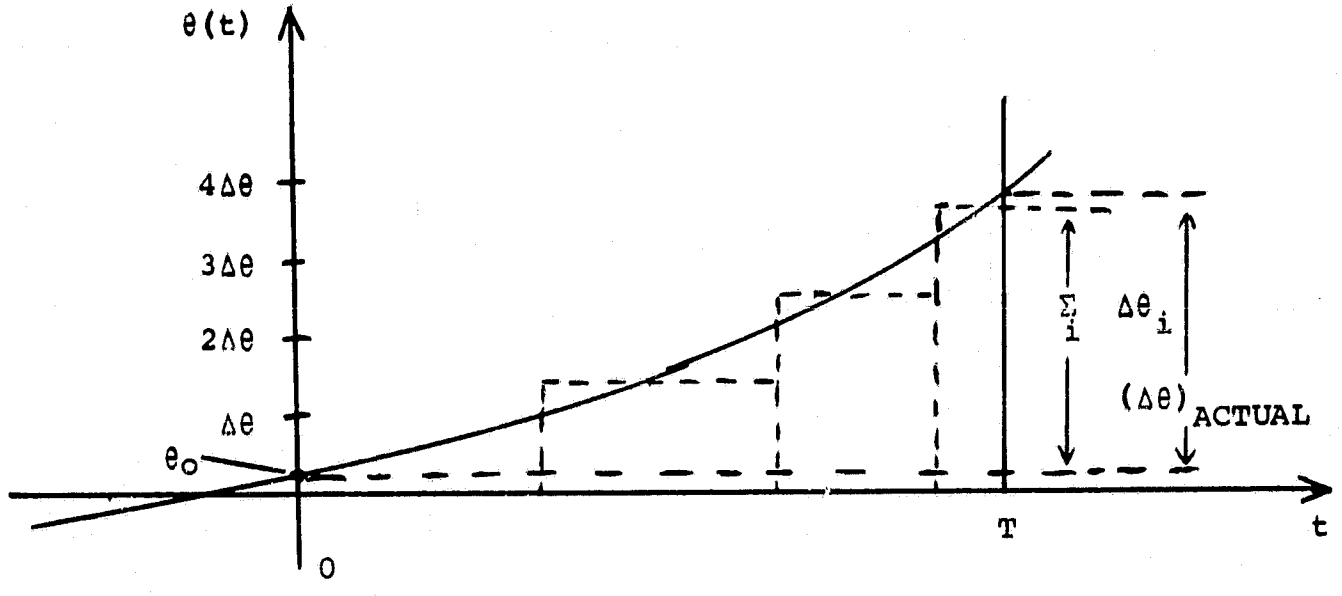

Figure A-1 Quantization Model

deriving rate is

$$\omega_{IND} = \frac{1}{T} \sum_{i} \Delta\theta_i \qquad \text{(A-1)}$$

with the $\Delta\theta_i$ summed over an interval T. The difference between the actual change in θ ($\Delta\theta_{ACTUAL}$) and the sum of the pulses ($\sum_i \Delta\theta_i$) can lie anywhere between $-(\Delta\theta - \theta_o)$ and θ if the initial angle is θ_o relative to a pulse point. These values are equally likely and so are defined by a uniform distribution,

$$P(e|\theta_o) = \frac{1}{\Delta\theta} \qquad [-(\Delta\theta - \theta_o) < e < \theta_o]. \tag{A-2}$$

But the initial value may also be considered uniformly distributed over 0, $\Delta\theta$:

$$P(\theta_o) = \frac{1}{\Delta\theta} \qquad (0 < \theta_o < \Delta\theta). \tag{A-3}$$

The mean quantization error is then

$$\overline{e}_{\omega\text{-quant}} = \frac{1}{T} \int d\theta_o \int de\ e\ P(e|\theta_o)P(\theta_o). \tag{A-4}$$

Using Equations A-2 and A-3 in A-4 we find the

$$\overline{e}_{\omega\text{-quant}} = 0 \tag{A-5}$$

as expected. The mean squared error, equal to the variance in this case, is

$$\overline{e^2}_{\omega\text{-quant}} = \frac{1}{T^2} \int d\theta_o \int de\ e^2\ P(e|\theta_o)P(\theta_o). \tag{A-6}$$

Evaluating Equation A-6 we find that

$$\overline{e^2}_{\omega\text{-quant}} = \frac{1}{6} \frac{\Delta e^2}{T^2}. \tag{A-7}$$

The differencing period, T, must be restricted to give the desired bandwidth in rate indication.

APPENDIX B

RELATIONSHIP BETWEEN RMS DEVIATION AND CRYSTAL OSCILLATOR PULLING RANGE

If a crystal is assumed to have a resonance-type characteristic, the admittance can be represented as

$$Y(\omega) = Y_o \left[\frac{\omega/\omega_o}{(\omega/\omega_o) + j\, Q\left[(\omega/\omega_o)^2 - 1\right]} \right]$$

and

$$< Y(\omega) = \tan^{-1} \left[- \frac{Q\left[(\omega/\omega_o)^2 - 1\right]}{\omega/\omega_o} \right].$$

We now approximate this by a straight line (near $\omega = \omega_o$) by Taylor series:

$$d(\tan^{-1} u) = \frac{du}{u^2 + 1}$$

$$\therefore \frac{d}{d\omega}[< Y(\omega)] \doteq \frac{-1}{1 + \frac{Q^2}{\omega^2\, \omega_o^2} (\omega^2 - \omega_o^2)} \cdot \frac{Q(\omega_o^2 + \omega^2)}{\omega^2\, \omega_o}$$

In the limit as $\omega \longrightarrow \omega_o$,

$$\frac{d}{d\omega}[< Y(\omega)] = -\frac{2Q}{\omega_o}$$

or

$$< Y(\omega) = \int_{\omega_o}^{\omega} \left(-\frac{2Q}{\omega_o}\right) d\omega$$

and the approximation for $< Y(\omega)$ becomes

$$< Y(\omega) = 2Q\left(1 - \frac{\omega}{\omega_o}\right).$$

If the phase limits for sustaining oscillation are $\pm \phi_m$, then the maximum pulling range is given by

$$\omega_p = \omega_o - \omega(\phi_m) = \omega_o - \left(1 - \frac{\phi_m}{2Q}\right)\omega_o$$

$$\omega_p = \frac{\phi_m \omega_o}{2Q} .$$

If we now assume (see Reference 2-6)

$$\Delta \simeq \frac{f_o}{Q}\sqrt{\frac{N}{P}}$$

where

Δ = rms frequency deviation

P = power,

N = kTB with k = Boltzmann's constant,

T = effective absolute temperature and

B = oscillator bandwidth,

then we get the ratio,

$$\frac{f_p}{\Delta} = \frac{\omega_p/2\pi}{\Delta} = \frac{\phi_m}{2\sqrt{N/P}} .$$

It can now be seen that the ratio of maximum pulling distance to RMS frequency deviation is a constant for a particular oscillator type or circuit.

APPENDIX C

HIGH RESOLUTION ANGULAR SENSOR TESTING USING COUNTER SYSTEMS

REFERENCES:

(1) "A High Resolution Laser Gyro Technology Development Program" Raytheon Company/Equipment Division ER75-4438-1, 8 December 1975. Submitted to Marshall Space Flight Center.

(2) J. Barnes, A. Chi, L. Cutler, D. Healey, D. Leeson, T. McGunigal, J. Mullen, Jr., W. Smith, R. Sydnor, R. Vessot and G. Winkler "Characterization of Frequency Stability" IEEE Transactions on Instrumentation and Measurement, Vol. IM-20, No. 2, May 1971, pp. 105 - 120.

(3) Hewlett-Packard Company Preliminary Specification on 5390A Frequency Stability Analyzer dated May 1976.

(4) Richard A. Baugh "Frequency Modulation Analysis With the Hadamard Variance" in Proceeding of the 25th Annual Frequency Control Symposium, Washington, D.C., April 1971. Also see AD-746211.

(5) Holly M. Cole "Time Domain Measurements" Countermeasures, August 1975, pp. 38 - 42,55.

1. INTRODUCTION

This memo discusses the applicability of counter systems, consisting of high precision counters and computing capability, to the efficient testing of high resolution laser gyros for accuracy. Two counter systems that have been considered for use are the currently available HP 5360A computing counter and the HP 5390A Frequency Stability Analyzer which is expected to be available in November. The counter used in the latter system is currently available as the HP 5345A.

2. MEASUREMENT CONSIDERATIONS

Organizations that are interested in the stability of frequency standards (oscillators, Cesium beams, Rubidium gas cells, masers, etc.) utilize a test that is recommended by NBS (National Bureau of Standards) for the determination of short-term stability. Short-term stability is considered the random perturbation from the nominal carrier frequency that is caused by noise. The NBS recommended test is a time domain test based on calculation of the so-called Allan Variance or RMS Fractional Frequency Deviation. Both systems can be used to calculate the Fractional Frequency Deviation, the 5360A by way of a plug-in keyboard and the 5390A by using a cassette in the HP 9825A calculator.

The Frequency Deviation measurement can also be applied to measuring the accuracy of the high resolution laser gyro by measurements of Δf where Δf is the four-frequency combination

$$\Delta f = \Delta f_1 - \Delta f_2 = (f_2 - f_1) - (f_4 - f_3). \qquad (1)$$

The Frequency Deviation measurement of this gyro signal will give the variation around the long-term components (bias and constant Earth rate). Thus the recommended test will give a measure of the inaccuracy of the system due to such causes as base vibrations, intrinsic gyro noise, quantization, phase lock loop short-term noise, etc. The Allan Variance approach is discussed in the next section.

3. ALLAN VARIANCE AND FRACTIONAL FREQUENCY DEVIATION

The classical formula for variance is given by

$$\sigma_N^2 = \frac{1}{N-1}\left[\sum_{i=1}^{N} f_i^2 - \frac{1}{N}\left(\sum_{i=1}^{N} f_i\right)^2\right]. \tag{2}$$

It has been found that the above formula does not always converge as the number of samples (N) increases. This has been traced to a type of noise (flicker noise) exhibited by most frequency sources. if, however, one sets N = 2,

$$\sigma_2^2 = \frac{(f_1 - f_2)^2}{2} \tag{3}$$

and the averaged value of σ_2 is

$$< \sigma_2 > = \sqrt{\frac{1}{2N}\sum_{i=1}^{N}\left(f_{2i} - f_{2i-1}\right)^2} \tag{4}$$

where N is now the number of successive pairs of measurements. The latter formula is the square root of the Allan Variance and does not diverge with N. By dividing by f_o, the nominal source frequency, we get for the RMS Fractional Frequency Deviation

$$< \sigma_2(\delta f/f_o) > \approx \frac{1}{f_o}\sqrt{\frac{1}{2N}\sum_{i=1}^{N}\left(f_{2i} - f_{2i-1}\right)^2} \quad . \tag{5}$$

The f's in this formula are averaged over a specific time interval say τ.

For gyro measurements we would multiply the results by f_o and convert from hertz to say $\widehat{sec}$/sec. By plotting this result versus the frequency averaging time τ we would get plots equivalent to that shown in Reference 1 (pg. 2-7). The Raytheon data taken for the latter plot was based upon summing of pulses for various times.

4. POWER SPECTRAL DENSITIES

Power spectral density measurement gives more information than the time domain RMS Fractional Frequency Deviation measurements discussed in Section 3. Power spectral density (PSD) measurements can be made with the 5390A Frequency Stability Analyzer but not with the 5360A Computing Counter. The method used by the 5390A to get PSD measurements will be discussed in the next section. In lieu of measurements by a system such as the 5390A one may infer PSD's from the data available from FFD (Fractional Frequency Deviation) measurements as is discussed next.

Consider a signal generator whose instantaneous output voltage may be written as

$$V(t) = [V_o + \varepsilon(t)]\sin[2\pi \nu_o t + \phi(t)] \qquad (6)$$

where V_o and ν_o are the nominal amplitude and frequency, respectively, of the output. Provided that $\varepsilon(t)$ and $\dot{\phi}(t) = d\phi/dt$ are sufficiently small for all time t, one may define the fractional instantaneous frequency deviation from the nominal by the relation

$$y(t) = \frac{\dot{\phi}(t)}{2\pi\nu_o} \quad . \qquad (7)$$

The PSD of y may be denoted by $S_y(f)$ and the following relations hold,

$$S_y(f) = \left(\frac{1}{2\pi\nu_o}\right)^2 S_{\dot{\phi}}(f) \qquad [8]$$

$$S_y(t) = \left(\frac{1}{\nu_o}\right)^2 f^2 S_{\phi}(f). \qquad [9]$$

It has been shown in Reference (2) that the average value of $\sigma_y^2(N,T,\tau) = < \sigma_y^2(N,\tau,\tau) >$ where

N = number of samples

T = time interval between the beginnings of two successive measurements of average frequency

τ = duration of averaging period of y(t) to obtain the $\overline{y_k}$ where

$$\overline{y_k} = \frac{1}{\tau}\int_{t_k}^{t_k+\tau} y(t)dt = \frac{\phi(t_k + \tau) - \phi(t_k)}{2\pi\ \nu_o\ \tau}$$

is given by

$$<\sigma_y^2(N,T,\tau)> = \frac{N}{(N-1)}\int_o^\infty df\ S_y(f)\frac{\sin^2(\pi f\tau)}{(\pi f\tau)^2}\left\{1 - \frac{\sin^2(\pi N f T)}{N^2\sin^2(\pi f T)}\right\}. \qquad (10)$$

The Allan variance used in the 5360A and 5390A is gotten from $\langle\sigma_y^2(2,T,\tau)\rangle$ by setting N = 2 and T = τ and thus the relation between Allan variances and $S_y(f)$ is given by

$$\text{Allan variance} = \sigma_y^2(\tau) = \langle\sigma_y^2(2,\tau,\tau)\rangle =$$

$$= 2\int_0^\infty df\, S_y(f)\frac{\sin^2(\pi f\tau)}{(\pi f\tau)^2}\left\{1 - \frac{\sin^2(2\pi f\tau)}{4\sin^2(\pi f\tau)}\right\}. \qquad (11)$$

If we make assumptions about the structure of $S_y(f)$, founded on experimental work, we can derive numerical results from the above relationship.

One type of noise that is common to most oscillators is flicker noise in frequency which is represented by

$$S_y(f) = \frac{h_{-1}}{f}. \qquad (12)$$

Using Eq. (12) in Eq. (11) it can be shown that

$$\sigma_y^2(\tau) = (2\ \ell n 2)h_{-1} \qquad (13)$$

and thus the numerical value of h_{-1} can be determined from the Allan variance data which will of course be constant with the averaging time τ. Other assumptions about the structure of $S_y(f)$ can be used to get PSD information from Allan variance relationship (Eq. 11). Appendix II of Reference (2) contains a good deal of information of this nature such as a random walk y with

$$\text{PSD } S_y(f) = \frac{h_{-2}}{f^2} \text{ etc.}$$

Rather than inferring PSD's as above from Allan variance measurements from the 5360A system, Hewlett-Packard has developed the 5390A Frequency Stability Analyzer to get direct measurements of the phase noise (equivalent to angular noise in gyro terms) PSD $S_{\phi}(f)$ which is related to the frequency deviation noise (equivalent to angular rate noise in gyro terms) $S_y(f)$ by the relationship given in Eq. (9). The method that is used in the 5390A system to measure $S_{\phi}(f)$ directly is discussed in the next section.

5. DIRECT MEASUREMENT OF PHASE NOISE POWER SPECTRAL DENSITIES

The information presented here has been gathered from References (3) - (5). The 5390A system can be used as a phase sensitive spectrum analyzer in the frequency domain allowing the operator to specify the offset frequencies (frequency offset from the carrier) at which measurements are to be made and to specify a bandpass bandwidth with which the observation will be made.

The so-called Hadamard variance is computed by the calculator (9825A). The Hadamard variance is the mean squared value of say k sequences of 2N values of the fractional frequency deviations y given by

$$m_1 = (y_{1.1} - y_{1.2}) + (y_{1.3} - y_{1.4}) + \ldots + (y_{1.2N-1} - y_{1.2N})$$

$$m_2 = (y_{2.1} - y_{2.2}) + (y_{2.3} - y_{2.4}) + \ldots + (y_{2.2N-1} - y_{2.2N})$$

$$\vdots$$

$$m_k = (y_{k.1} - y_{k.2}) + (y_{k.3} - y_{k.4}) + \ldots + (y_{k.2N-1} - y_{k.2N}) \qquad (14)$$

The calculator then computes the Hadamard variance of the m_k sums using

$$\sigma_H^2\left(\tau_m, \tau_D, K\right) = \frac{1}{K-1}\left[\sum_{i=1}^{K} m_i^2 - \frac{1}{K}\left(\sum_{i=1}^{K} m_i\right)^2\right] \qquad (15)$$

where,

τ_m = measurement interval for each value of y

τ_d = dead-time between each value of y

K = number of m sequences

The 2N samples of y in each sequence are gated from the counter into the calculator by N cycles of the sampling function in the sketch below:

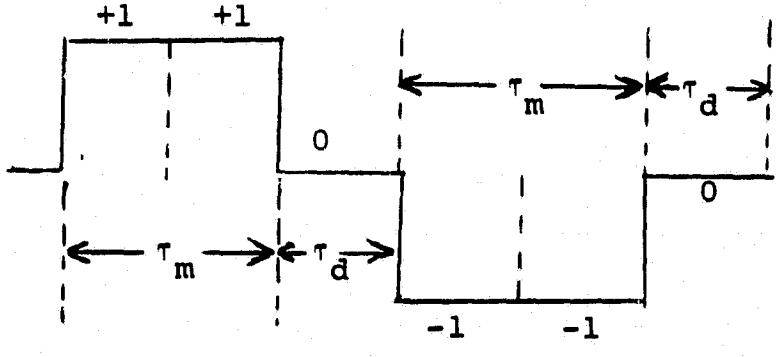

Each cycle is divided into six segments. Weighting functions, a_i, are applied to each measurement by allowing a_1 and $a_2 = +1$, a_3 and $a_6 = 0$, and a_4 and $a_5 = -1$. This is physically implemented by setting the measurement time τ_m, equal to twice the dead time, τ_d. The choice of 50% dead time is the best approximation (closer to a sine wave) than any other choice. The transfer function for ten cycles of the above sampling function with $\tau_d = 0$ is shown in Figure 1.

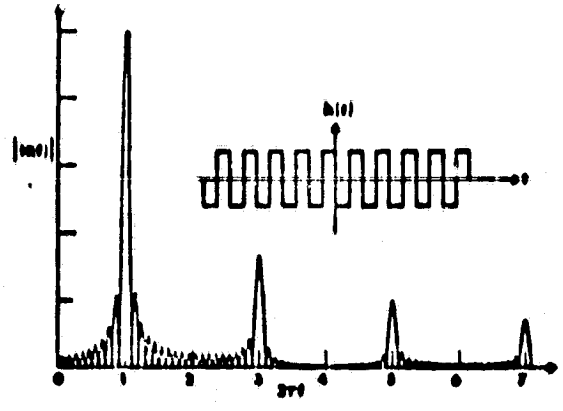

Figure 1 The Hadamard Variance Transfer Function (N = 10)

The 50% dead time eliminates the third, ninth, fifteenth, etc. harmonics as shown in Figure 2.

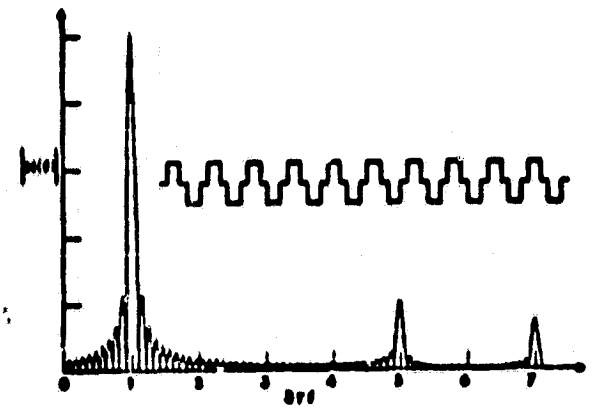

Figure 2 The Modified Hadamard Variance Transfer Function (50% Dead Time, N = 10)

The counters' transfer function, corresponding to a sampling function as shown in Figure 2, can be represented by

$$H(f) = \frac{\sin(\pi f \tau_m)}{\pi f \tau_m} \cdot \frac{\sin 2Nf(\tau_m + \tau_d)}{\cos \pi f(\tau_m + \tau_d)} \qquad (16)$$

The filter function, H(f), of the counter can be made to appear as a very narrowband wave analyzer in the frequency domain. The center frequency of H(f) is controlled by selecting the measurement time, τ_m, and the dead time, τ_d, such that

$$f = \frac{1}{2(\tau_m + \tau_d)} \qquad (17)$$

and the bandwidth, B, of the measurement may be controlled by varying the number of measurement pairs, N, such that

$$B = \frac{f}{N} \quad . \qquad (18)$$

We may relate the Hadamard variance of Eq. (15) to the phase power spectral density, S_ϕ, by

$$\sigma_H^2(\tau_m, \tau_d, K) = 2\pi \int_{-\infty}^{\infty} |H(f)|^2 f^2 S_\phi(f) df. \qquad (19)$$

By using the approximation that the H(f) is a delta function at the selected frequency (f_o) we get that

$$S_\phi(f_o) = \frac{\sigma_H^2}{(2\pi) f_o^2 |H(f_o)|^2} \qquad (20)$$

where $H(f_o)$ is computed from Eq. (16). The system plotter (9871A Printer-Plotter) gives a log-log plot of the ratio of single side band phase noise to the carrier noise power in db/Hz vs. the offset frequency from the carrier in Hertz. In the case of gyro measurements the phase power spectral density is equivalent to the angular power spectral density. If the calculator program is altered slightly we can get the angular rate power spectral density by multiplying the angular PSD by f^2. The integral under the PSD curve gives the overall RMS angular error or the overall RMS angular rate error of the instrument.

For the high resolution angular sensor we are interested in frequencies below 10 Hertz. The wave analyzer range of operation is from a couple of Hertz up high frequencies. The sensitivity of the digital counter below ten Hertz is superior to the sensitivity of a wave analyzer over its range. We must be prepared to make measurements down to 0.01 or perhaps 0.001 Hertz. Thus the 5390A Frequency

Stability Analyzer is an ideal test instrument for our application. Fast results using only a single instrument would be attainable. In a production situation such an instrument would certainly make up for its high cost, expected to be in the $25,000 bracket.

6. SUMMARY OF COUNTER SYSTEMS

A. 5360A COMPUTING COUNTER

(1) Typical system consists of:

- Computing Counter 5360A
- Input Module 5365A
- Time Interval Plug-In 5379A
- Keyboard 5375A

(2) Five systems in Equipment Division. One newly repaired and calibrated system is being assigned to this contract for 1976.

(3) Input carrier frequency range:

- DC to 320 MHz

(4) Single channel input

(5) Measurement characteristics:

(a) Measurement resolution: one part in 10^{10} per second of gate time.

(b) Interpolator Error: $\pm 10^{-9}$ per second of measurement time.

(c) Relative error due to time base short term stability (see Figure 2-23, 5360A Computing Counter Training Manual). The short term stability $(\frac{\Delta f}{f})_{RMS}$ is less than 5×10^{-11} for a one-second averaging time.

(d) Long term stability (also called drift rate or aging rate) is 5×10^{-10} per day.

(e) Trigger error: see pages 43 - 46 of Training Manual.

(6) Frequency Measurement Range:
0.01 Hz to 320 MHz.

(7) Computes short term stability data using Allan variances using Program #7.

(8) Cannot be used to measure power spectral densities. Inferences must be made to relate the Allan variance slopes to slopes of the power spectral density.

B. 5390A FREQUENCY STABILITY ANALYZER

(1) System expected to be configured as follows:

5390A BASIC SYSTEM

5345A	Option 011
5358A	Measurement Storage Plug-in
10830A	Signal Conditioner/Mixer
10831A	Tone Generator
9825A	Calculator
98210A	Adv. Program/String Variab. ROM
98213A	Gen. I/O/Extended I/O ROM
98034A	HP-IB Interface
9871A	Option 001 Printer/Plotter
05390-80025	Systems Interface Kit

Cassette and operational software for 9825A; Includes RMS Fractional Frequency Deviation (Allan Variance) and Phase Spectral Density (phase noise) programs; HP-IB cables; BNC cables; Tee; System Manual; Technical Handbook; and Diagnostic procedures.

System Cabinet

Factory assembly and integration prior to shipment.

90 day on-site calculator product warranty.

1 year bench repair instrument warranty.

(2) Expected price: $25,500.

(3) Availability: November 1976.

(4) Input carrier frequency range to 10830A mixer/IF amplifier: 500 KHz to 18 GHz. Also excepts external IF signal through rear input of 1 Hz to 100 KHz. The 10830A does not handle the carrier frequency range from 100 KHz to 300 KHz but HP has an option unit (old, designation unknown) that handles the range from 50 KHz to 150 MHz.

(5) Range of offset frequency from carrier, f, to IF frequency, f_{IF} (see Figure 3 of Reference 3). Applies to phase spectral density measurements.

f_{IF}	Range of f
10.0 Hz	0.01 Hz to 1.67 Hz
100.0 Hz	0.01 Hz to 16.7 Hz
1.0 KHz	0.01 Hz to 167.0 Hz
10.0 KHz	0.01 Hz to 1.67 KHz
66.67 KHz	0.01 Hz to 11.1 KHz

(6) Short Term Stability Measurements

(a) Employs the Allan Variance to monitor short term stability for different averaging times in the time domain. Very similar to HP Application Note 174-7 with the noted exception that dead time between measurements become insignificant for averaging times down to 1 msec.

(b) Minimum dead time is one period of input frequency or [7.0 + (1.6X number of digits stored)] μsec. whichever is greater.

(c) Resolution - see HP Application Note 174-7. The RMS resolution limit of the 5345 counter is 8.2×10^{-10} per second of gate time.

(7) Phase Spectral Density Measurements

(a) Direct measurement of phase noise power spectral densities (see Section 5).

(b) Accuracy

Since measurements are actually made on zero crossings in the time domain, measurement calibration of the signal's carrier level in the frequency domain is not necessary. The value of the phase noise being measured is actually a random variable rather than an absolute value, hence, the measurements are statistical in nature and result in an estimate of the mean value of phase noise during the observation period. The 1σ values are given along with the estimated mean to indicate the confidence value of the measurement. Longer observation periods will increase the level of confidence.

(c) Sensitivity

System sensitivity in Dbc can be expressed in terms of the offset frequency from the carrier, f, desired and the IF frequency, f_{IF}, used by the following relationship:

Sensitivity in Dbc = $-173 + 20 \log f_{IF} - 10 \log f$.
Also refer to Figure 3 of Reference 3.

7. CONCLUSIONS

Both the 5360A Computing Counter and the 5390A Frequency Stability Analyzer can be used to check the accuracy of the high resolution angular sensors. Both systems will give the desired data but the 5390A system will be more direct and efficient especially for any future production testing of laser gyros.

Since the quantization problem appears to be solved it should be possible, at this time, to distinguish whether base vibrations or gyro noise (intrinsic gyro noise plus phase-lock loop component noise) are dominant. If it turns out that base vibrations are masking the gyro noise it will be necessary to move the gyro tests to a quieter environment. Since a Computing Counter is being made available to us for the rest of the year, it is recommended that some early tests be made to assess the suitability of the tests and to determine, for future planning purposes, whether base vibration will interfere with accuracy testing.

APPENDIX D

OPERATING FREQUENCIES AND COUNTDOWN RANGES OF THE HIGH RESOLUTION CIRCUITRY

APPENDIX D

OPERATING FREQUENCIES AND COUNTDOWN RANGES OF THE HIGH RESOLUTION CIRCUITRY

Δf_1 or Δf_2	$\pm f$	Division Factor	*Countdown Ratio
1029411.76	38.24	68.00	17.00
972222.22	36.11	72.00	18.00
921052.63	34.21	76.00	19.00
875000.00	32.50	80.00	20.00
833333.33	30.95	84.00	21.00
795454.55	29.55	88.00	22.00
760869.57	28.26	92.00	23.00
729166.67	27.08	96.00	24.00
700000.00	26.00	100.00	25.00
673076.92	25.00	104.00	26.00
648148.15	24.07	108.00	27.00
625000.00	23.21	112.00	28.00
603448.28	22.41	116.00	29.00
583333.33	21.67	120.00	30.00
564516.13	20.97	124.00	31.00
546875.00	20.31	128.00	32.00
530303.03	19.70	132.00	33.00
514705.88	19.12	136.00	34.00
500000.00	18.57	140.00	35.00
486111.11	18.06	144.00	36.00
472972.97	17.57	148.00	37.00
460526.32	17.11	152.00	38.00
448717.95	16.67	156.00	39.00
437500.00	16.25	160.00	40.00
426829.27	15.85	164.00	41.00
416666.67	15.48	168.00	42.00
406976.74	15.12	172.00	43.00
397727.27	14.77	176.00	44.00
388888.89	14.44	180.00	45.00
380434.78	14.13	184.00	46.00

*The division factor is set into the frequency divider set switches by subtracting the appropriate number in the countdown ratio column from 256 and setting the resulting number in digital form into the switches.

Δf_1 or Δf_2	$\pm f$	Division Factor	*Countdown Factor
372340.43	13.83	188.00	47.00
364583.33	13.54	192.00	48.00
357142.86	13.27	196.00	49.00
350000.00	13.00	200.00	50.00
343137.25	12.75	204.00	51.00
336538.46	12.50	208.00	52.00
330188.68	12.26	212.00	53.00
324074.07	12.04	216.00	54.00
318181.82	11.82	220.00	55.00
312500.00	11.61	224.00	56.00
307017.54	11.40	228.00	57.00
301724.14	11.21	232.00	58.00
296610.17	11.02	236.00	59.00
291666.67	10.83	240.00	60.00
286885.25	10.66	244.00	61.00
282258.06	10.48	248.00	62.00
277777.78	10.32	252.00	63.00
273437.50	10.16	256.00	64.00
269230.77	10.00	260.00	65.00
265151.52	9.85	264.00	66.00
261194.03	9.70	268.00	67.00
257352.94	9.56	272.00	68.00
253623.19	9.42	276.00	69.00
250000.00	9.29	280.00	70.00
246478.87	9.15	284.00	71.00
243055.56	9.03	288.00	72.00
239726.03	8.90	292.00	73.00
236486.49	8.78	296.00	74.00
233333.33	8.67	300.00	75.00
230263.16	8.55	304.00	76.00
227272.73	8.44	308.00	77.00
224358.97	8.33	312.00	78.00
221518.99	8.23	316.00	79.00
218750.00	8.13	320.00	80.00
216049.38	8.02	324.00	81.00
213414.63	7.93	328.00	82.00
210843.37	7.83	332.00	83.00

RAYTHEON COMPANY
EQUIPMENT DIVISION
RAYTHEON

Δf_1 or Δf_2	$\pm f$	Division Factor	*Countdown Factor
208333.33	7.74	336.00	84.00
205882.35	7.65	340.00	85.00
203488.37	7.56	344.00	86.00
201149.43	7.47	348.00	87.00
198863.64	7.39	352.00	88.00
196629.21	7.30	356.00	89.00
194444.44	7.22	360.00	90.00
192307.69	7.14	364.00	91.00
190217.39	7.07	368.00	92.00
188172.04	6.99	372.00	93.00
186170.21	6.91	376.00	94.00
184210.53	6.84	380.00	95.00
182291.67	6.77	384.00	96.00
180412.37	6.70	388.00	97.00
178571.43	6.63	392.00	98.00
176767.68	6.57	396.00	99.00
175000.00	6.50	400.00	100.00
173267.33	6.44	404.00	101.00
171568.63	6.37	408.00	102.00
169902.91	6.31	412.00	103.00
168269.23	6.25	416.00	104.00
166666.67	6.19	420.00	105.00
165094.34	6.13	424.00	106.00
163551.40	6.07	428.00	107.00
162037.04	6.02	432.00	108.00
160550.46	5.96	436.00	109.00
159090.91	5.91	440.00	110.00
157657.66	5.86	444.00	111.00
156250.00	5.80	448.00	112.00
154867.26	5.75	452.00	113.00
153508.77	5.70	456.00	114.00
152173.91	5.65	460.00	115.00
150862.07	5.60	464.00	116.00
149572.65	5.56	468.00	117.00
148305.08	5.51	472.00	118.00

RAYTHEON COMPANY
EQUIPMENT DIVISION
RAYTHEON

Δf_1 or Δf_2	$\pm f$	Division Factor	*Countdown Factor
147058.82	5.46	476.00	119.00
145833.33	5.42	480.00	120.00
144628.10	5.37	484.00	121.00
143442.62	5.33	488.00	122.00
142276.42	5.28	492.00	123.00
141129.03	5.24	496.00	124.00
140000.00	5.20	500.00	125.00
138888.89	5.16	504.00	126.00
137795.28	5.12	508.00	127.00
136718.75	5.08	512.00	128.00

C-2

RAYTHEON COMPANY
EQUIPMENT DIVISION

RAYTHEON

APPENDIX E

SPECIFICATION FOR THE VOLTAGE CONTROLLED OSCILLATORS USED IN THE HIGH RESOLUTION CIRCUITRY

APPLICATION		REVISIONS				
NEXT ASSY	USED ON	LTR	DESCRIPTION		DATE	APPROVED
		A	SH1 UPDATED REVISION STATUS SH2 REVISED EXTENSIVELY		22 SEP72	ECH
		B	SEE SECO 15304	LT	8NOV72	ECH
		C	SEE SECO 15321	WEB	24JAN73	
		D	SEE SECO 15349	WEB	12APR73	
		E	SEE SECO-15442	RM	19NOV73	

PREPARED IN ACCORDANCE
WITH MIL-STD-10CA

REV STATUS OF SHEETS	REV LTR	E	D	E	C										SPECIFICATION CONTROL DRAWING
	SHEET NO.	1	2	3	4										

UNLESS OTHERWISE SPECIFIED DIMENSIONS ARE IN INCHES
TOLERANCES: ANGLES ±
FRACTIONS ±
3 PLACE DECIMALS ±.005
2 PLACE DECIMALS ±.02
1 PLACE DECIMALS ±

MATERIAL:

CONTR NO.

DR: L. Thomson 14SEP'72
CH: C.K. Stahl 15SEP72
APP'D: R. Gilcease 25SEP 72

APPROVED 394

BY DIRECTION OF

RAYTHEON

RAYTHEON COMPANY
LEXINGTON, MASS. 02173

DRAWING TITLE

OSCILLATOR, RADIO FREQUENCY

SIZE	CODE IDENT NO.	DRAWING NO.
A	49956	735756

SCALE NONE SHEET 1 OF 4

-1

1. DESCRIPTION: OSCILLATOR, CRYSTAL, VOLTAGE CONTROLLED AND TEMPERATURE COMPENSATED.

2. THIS OSCILLATOR SHALL MEET THE REQUIREMENTS OF MIL-O-55310 FOR CLASS 5 WITH THE FOLLOWING MODIFICATIONS AND ADDITIONS:

3. ELECTRICAL REQUIREMENTS:

3.1 OUTPUT FREQUENCY: SEE TABLE I.

3.2 OSCILLATOR SUPPLY VOLTAGE: +15 VOLTS DC ± 1.0%.

3.3 MODULATION INPUT VOLTAGE: 0.0 ± 3.5 VOLTS DC.

3.4 OSCILLATOR INPUT POWER: NOT TO EXCEED 0.5 WATT.

3.5 OUTPUT VOLTAGE: 1.0 VOLT PEAK TO PEAK MINIMUM INTO 1000 OHMS.

3.6 OUTPUT WAVEFORM: SINE WAVE.

3.7 SPURIOUS RESPONSE: 40.0 DECIBELS DOWN MINIMUM FROM MAIN RESPONSE.

3.8 MINIMUM FREQUENCY PULL RANGE: SEE TABLE I.

3.9 DEVIATION SENSITIVITY: SEE TABLE I.

3.10 DEVIATION LINEARITY: ± 20%.

3.11 AGING: $\pm 1 \times 10^{-6}$ MAXIMUM PER MONTH FOR AN OPERATING LIFE OF 10 YEARS AT A MODULATION INPUT VOLTAGE OF 0.0 VOLT DC.

3.12 FREQUENCY STABILITY: $\pm 1 \times 10^{-6}$ OVER THE TEMPERATURE RANGE OF 0°C TO 55°C AFTER 30 MINUTE WARM UP AT 0.0VOLT MODULATION INPUT.

4. MECHANICAL REQUIREMENTS:

4.1 CONSTRUCTION CASED, SEALED.

4.2 MOUNTING: BY PRINTED CIRCUIT PINS.

4.3 TERMINALS: SHALL MEET SOLDERABILITY REQUIREMENTS OF MIL-STD-202 METHOD 208.

4.4 AGING ADJUST: SEE FIGURE 1.

4.5 FINISH: NICKEL PLATE

5. ENVIRONMENTAL REQUIREMENTS: PER MIL-O-55310 WITH THE FOLLOWING MODIFICATIONS AND ADDITIONS:

5.1 AMBIENT TEMPERATURE RANGE:

SIZE	CODE IDENT NO.	DRAWING NO.
A	49956	735756
SCALE NONE	REV -	SHEET 2

BRUNING 15705

10-0703 CONT (5/68) VELLUM
10-0704 CONT (5/68) GRID VELLUM
10-0705 CONT (5/68) FILM PRINTED IN U.S.A.

5.1.1 OPERATING: 0°C TO 55°C.

5.1.2 NON OPERATING: -54°C TO +70°C.

5.2 ALTITUDE:

5.2.1 OPERATING: 10,000 FEET MAXIMUM.

5.2.2 NON OPERATING: 40,000 FEET MAXIMUM.

5.3 VIBRATION: PER MIL-STD-810, METHOD 514, PROCEDURE X AND CURVE AW, 1.5 G'S MAXIMUM 5 TO 5000 HERTZ.

5.4 SHOCK PER MIL-STD-810, METHOD 516, PROCEDURE V.

6. MINIMUM OPERATING LIFE EXPECTANCY: 10 YEARS.

7. QUALITY ASSURANCE PROVISIONS: SHALL BE IN ACCORDANCE WITH THE REQUIREMENTS OF MIL-O-55310 EXCEPT THAT QUALIFICATION INSPECTION, FIRST ARTICLE INSPECTION AND GROUP B INSPECTION ARE NOT REQUIRED UNLESS SPECIFIED IN THE CONTRACT OR ORDER.

SUGGESTED SOURCE (S) OF SUPPLY:

MOTOROLA COMP DIV.
CHICAGO, ILL.
PART NO. SEE TABLE I.

TABLE I

RAYTHEON PART NO.	OUTPUT FREQUENCY MEGAHERTZ	FREQUENCY PULL RANGE MINIMUM	DEVIATION SENSITIVITY HERTZ/VOLT	MANUFACTURER'S PART NUMBER
735756-1	70.000000	$\pm 1 \times 10^{-5}$	200	K1085A-331-72-70MHZ
-2	39.321600	$\pm 5 \times 10^{-6}$	50	K1085A-331-72-39.3216MHZ
-3	70.000000	$\pm 5 \times 10^{-5}$	1000	K1085A-375-73-70MHZ
-4	5.00000	NONE	NONE	K1085A-4S1A

SIZE	CODE IDENT NO.	DRAWING NO.
A	49956	735756
SCALE NONE	REV E	SHEET 3

SHAPE OPTIONAL WITHIN LIMITS SHOWN

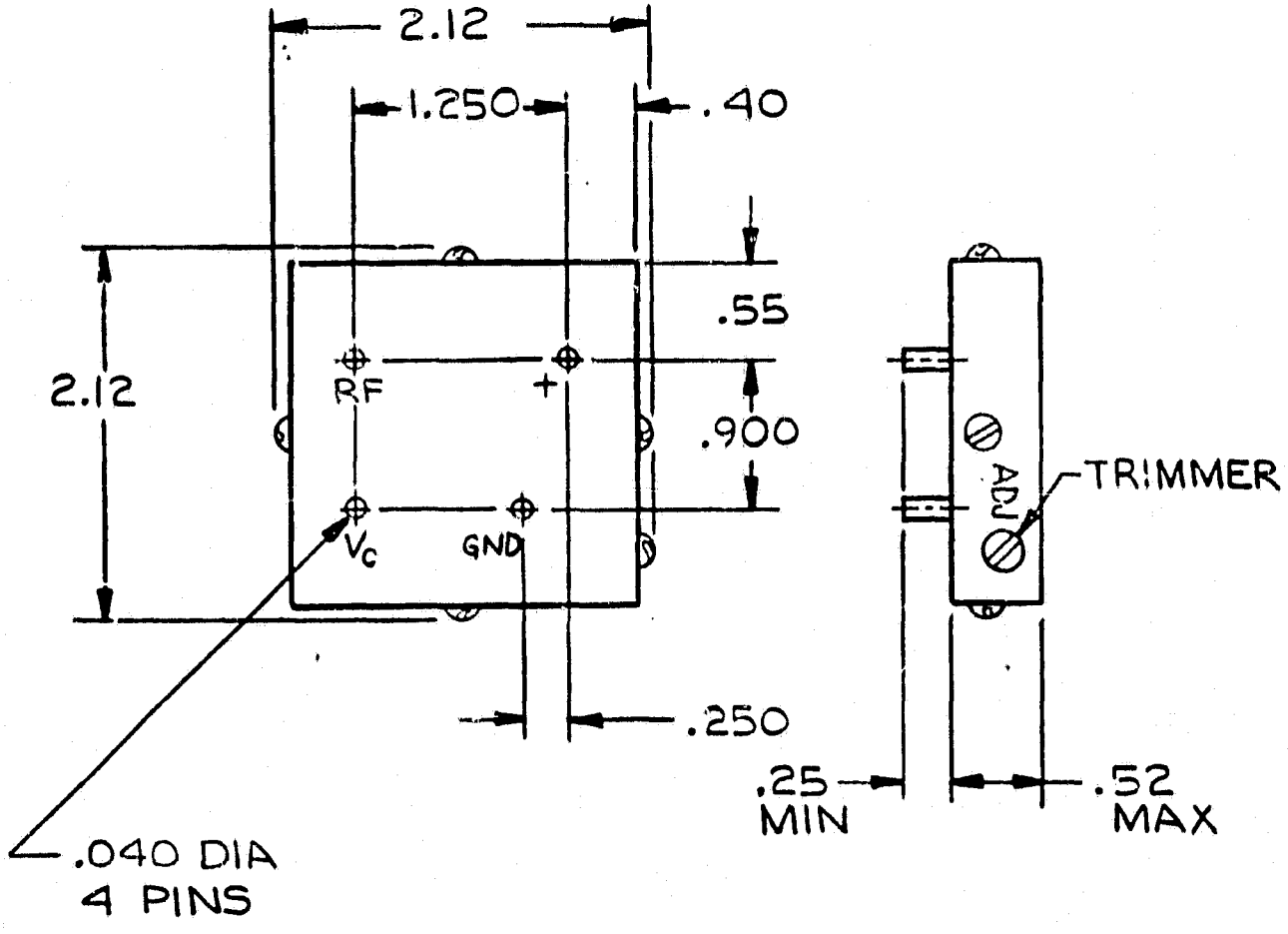

FIGURE 1

SIZE	CODE IDENT NO.	DRAWING NO.
A	49956	735756
SCALE 1/1	REV C	SHEET 4

APPENDIX F

RAYTHEON PROGRAMMING FOR THE 65 MHz BANDPASS FILTER AND PROJECTED RESPONSE

```
 77/09/23. 10.08.17.
PROGRAM   RODFIL

NUMBER OF SECTIONS
? 6
LOW PASS PARAMETER VALUES,  IN THE FORM-:
Q1 LOADED,INTERSTAGE COUPLING,QN LOADED
?.9372,.8088,.55,.5177,.55,.8088,.9372
PAUSE
?


  C
RATIO OF ACTUAL INTUCTANCE TO THEORETICAL INDUCTANCE
? .85
INPUT TERMINATING IMPEDANCE IN OHMS
? 50
OUTPUT TERMINATING IMPEDANCE IN OHMS
? 50
PERCENT BANDWIDTH
? 7
CENTER FREQUENCY IN MHZ
? 65
FORMER DIA IN INCHES
? .25
NUMBER OF TURNS PER COIL ON MIDDLE SECTIONS
? 10
NUMBER OF TURNS ON INPUT COIL
? 10
NUMBER OF TURNS ON OUTPUT COIL
? 10
COIL WINDING PITCH IN INCHES
? .0357
THE MIDDLE SECTION COIL Q FACTOR IS-:
       244
IF THIS Q IS HIGH ENOUGH TYPE1,IF NOT TYPE 0
? 1
MIDDLE SECTION TUNING CAP. IN PICOFARADS
    21.194
IF THIS IS A CONVENIENT CAPACITANCE VALUE TYPE 1
IF NOT TYPE 0,AND ADJUST COIL DIMEN. WHEN ASKED
? 21 *DEL*
1
```

FORMER DIAMETER	INPUT SERIES CAP.	INPUT SHUNT CAP.	OUTPUT SERIES CAP.	OUTPUT SHUNT CAP.	IN/OUTPUT IMPEDANCE
INCHES	PF	PF	PF	PF	OHMS
.250	8.950	12.533	8.950	12.533	50/ 50

IF THESE ARE CONVENIENT CAP VALUES TYPE 1
IF NOT TYPE 0 AND ADJUST END SECT. COIL DIMEN WHEN ASKED
? 1

IDENTIFICATION		WIDTH IN INCHES
COIL	1	.3570
SPACE	1	.0945
COIL	2	.3570
SPACE	2	.1509
COIL	3	.3570
SPACE	3	.1609
COIL	4	.3570
SPACE	4	.1509
COIL	5	.3570
SPACE	5	.0945
COIL	6	.3570

FORMER LENGTH IN INCHES
2.794

MIDDLE SECTION UNLOADED Q
244

WINDING PITCH IN INCHES
.0357000

```
THE FOLLOWING INDUCT VALUES ARE IN MICROHENRIES

INPUT INDUCT   MIDDLE INDUCT   OUTPUT INDUCT
      .283           .283            .283


 IDENTIFICATION        MUTUAL INDUT
       1                   .0159
       2                   .0108
       3                   .0102
       4                   .0108
       5                   .0159
PAUSE
? STOP
 *TER*
READY.
OLD,RSP/UN=R547102

READY.
RUN
```

```
 77/09/23. 10.15.15.
PROGRAM   RSP
NUMBER OF SECTIONS
? 6
INPUT AND OUTPUT CAP IN PICOFDS,IN THE FORM:
INPUT SERIES,INPUT SHUNT,OUTPUT SERIES,OUTPUT SHUNT
? .9,1,12,.9,1,12
MIDDLE SECTION TUNING CAPS IN PICOFDS , IN THE FORM:-
C1,C2,C3,.........CN THERE SHOULD BE TWO LESS CAPS
THAN THE NUMBER OF SECTIONS
? 22,22,22,22
INPUT RESISTANCE,OUTPUT RESISTANCE
? 50,50
FORMER DIA IN INCHES
? .25
NUMBER OF TURNS ON EACH COIL,COIL #1 FIRST
? 10,10,10,10,10,10
COIL WINDING PITCH IN INCHES
? .0357
DISTANCE BETWEEN COILS IN INCHES,SPACE#1 FIRST
? .0945,.15,.16,.15,.0945
DO YOU WISH TO CHANGE ANY PARAMETERS,TYPE 1 FOR YES,0 NO
? 0
COIL Q FACTOR
? 150
SHAPE FACTOR
? 1
RATIO OF THEORETICAL INDUCTANCE TO ACTUAL INDUCTANCE
? .85
LOW FREQ LIMIT,HIGH FREQ LIMIT,INCF  IN MHZ
? 60,70,.2
```

```
VERT SCALE IN DB PER POS.--INSERT.LOSS,RETURN LOSS
? 1,1
VERT SCALE- NANOSECS PER POS.
? 15
PLOT SYMBOLS-:  INSERT.LOSS(+)  RETURN LOSS(O)  DELAY(X)
COIL Q=250  NO. OF SECTS= 4  FORM DIA= .250
```

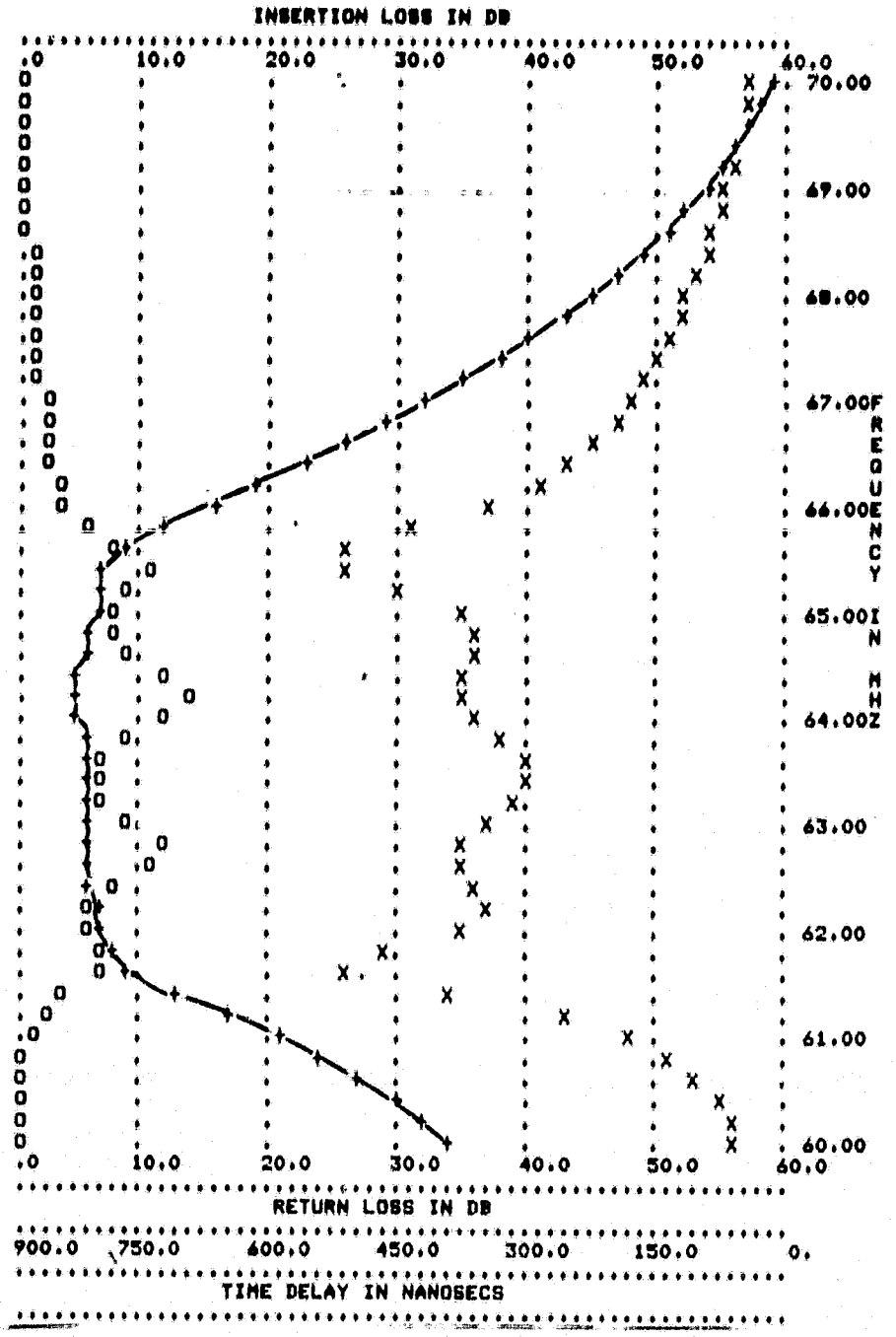

6.84512	93.65236
6.70541	87.90696
6.57379	82.24346
6.45047	76.65512
6.33579	71.13488
6.23026	65.67516
6.13460	60.26775
6.04982	54.90348
5.97733	49.57201
5.91910	44.26132
5.87792	38.95710
5.85781	33.64188
5.86471	28.29367
5.90769	22.88393
6.00114	17.37435
6.16911	11.71154
6.45441	5.81814
6.93926	-.42232
7.79711	-7.18965
9.43639	-14.75004
12.92322	-23.34368
20.91573	-31.89144
34.35164	-32.49244
36.93222	-23.44136
31.50536	-24.10089
30.87282	-30.78525
36.09901	-37.21071
45.82240	-38.15046
52.18702	-29.64967
46.84752	-20.89586
37.59490	-21.28025
31.92776	-27.46874
30.82669	-35.38136
34.29877	-42.77281
42.55698	-46.47019
51.68895	-40.92747
50.05233	-28.86246
39.02195	-24.79316
30.34368	-29.27707
27.15417	-36.24001
29.23042	-41.40347
33.06050	-38.88239
26.34506	-32.51056
15.92844	-35.92909
10.33557	-43.04620
7.63573	-49.74855
6.[illegible]25	-55.61490
5.31648	-60.82594
4.[illegible]3939	-65.56354
4.32856	-69.95454
4.01933	-74.08397

```
DO YOU WISH TO CHANGE ANY PARAMETERS,TYPE 1 FOR YES,0 NO
? STOP
```